Identification of a MYCN and Wnt-related VANGL2-ITLN1 fusion gene in neuroblastoma

Duffy, David; Konietzny, Anja; Krstic, Aleksandar; Mehta, Jai Prakash; Halasz, Melinda; Koch, Walter

Gene Reports

DOI:
10.1016/j.genrep.2018.06.018

Published: 01/09/2018

Identification of a MYCN and Wnt-related VANGL2-ITLN1 fusion gene in neuroblastoma.

David J. Duffy[1,2,3,4], **Anja Konietzny**[1,5], **Aleksandar Krstic**[1], **Jai Prakash Mehta**[1], **Melinda Halasz**[1,6] **& Walter Kolch**[1,6]

[1] Systems Biology Ireland, School of Medicine, University College Dublin, Belfield, Dublin 4, Ireland.
[2] The Whitney Laboratory for Marine Bioscience and Sea Turtle Hospital, University of Florida, St. Augustine, Florida 32080, USA.
[3] Molecular Ecology and Fisheries Genetics Laboratory, School of Biological Sciences, Bangor University, Bangor, Gwynedd LL57 2UW, UK.
[4] Department of Biological Sciences, School of Natural Sciences, Faculty of Science and Engineering, University of Limerick, Limerick, Ireland.
[5] Department of Biology, University of Konstanz, Konstanz, Germany.
[6] School of Medicine, University College Dublin, Belfield, Dublin 4, Ireland.

Correspondence to: David J. Duffy**.** Email: d.duffy@bangor.ac.uk

Running title: VANGL2-ITLN1 fusion gene in neuroblastoma

Key words: Neuroblastoma; MYCN; Wnt/β-catenin signalling pathway; Wnt/planar cell polarity (PCP) pathway; Precision Medicine; Genome Medicine; Genomic Rearrangements; Chromothripsis; RNA-seq; Genomics; fusion gene; ITLN; VANGL.

Abstract

The genomic fusion of two genes can lead to the expression of a fusion protein that can have oncogenic potential. The important contribution of such fusion genes to oncogenesis and tumour progression is being increasingly recognised. Here we report the presence of a novel VANGL2-ITLN1 fusion gene in the IMR32 neuroblastoma cell line. The fusion gene was identified by applying FusionHunter analysis to neuroblastoma cell line RNA sequencing data. This fusion results in the dramatic overexpression of a fusion transcript incorporating the full length ITLN1 coding sequence. Furthermore, the tumour expression levels of both components of the fusion gene (ITLN1 and VANGL2) are predictive of neuroblastoma patient outcome. High ITLN1 expression levels correlate with worse outcome across all neuroblastoma tumour stages and across MYCN amplification statuses. Survival probability was markedly worse for patients with both elevated MYCN and ITLN1 expression. We show that the VANGL2-ITLN1 fusion transcript can be transcriptionally upregulated upon lithium

chloride (LiCl) treatment, a known agonist of the Wnt signalling pathway. The novel VANGL2-ITLN1 fusion is associated with regulatory networks such as MYCN, ALK and the Wnt/Planar Cell Polarity (PCP) pathway which are key regulators of neuroblastoma outcome. We reveal novel putative multilevel-interactions between the fusion gene components and the MYCN oncogene, including MYCN ITLN protein-protein interactions. Through its interactions with other oncogenes the VANGL2-ITLN1 fusion gene is likely to be involved in driving neuroblastoma progression and poor patient outcomes.

Introduction

Many cancer cell types show inherently accelerated rates of mutation, which enables them to acquire selective advantages that drive tumour progression. Genomic instability, one of the major hallmarks of cancer, leads to random mutations, including chromosomal rearrangements and gene fusions. The fusion of two genes can lead to the expression of a fusion protein with oncogenic potential [1-5], such as the EWS-FL1 fusion in Ewing's sarcoma and the BCR-ABL fusion in leukaemia [6, 7]. Such fusion proteins are ideal potential targets for cancer treatment, since they do not occur in normal tissues. Alternatively, chromosomal translocation events can lead to the fusion of a proto-oncogene to a strong active promotor, or reduce the expression of a tumour suppressor gene by fusion to a silenced promoter, a promoter-less region, or by destroying the open reading frame.

Whole genome sequencing can be useful for detecting novel fusion genes. However, to determine whether predicted fusion genes are indeed expressed requires independent expression profiling, which can be challenging given the level of false positives which are called by current short read length sequencing methods. For example, in a study of putative chimeric genes in neuroblastoma, only 19% of chimeric genes identified by genomic DNA sequencing had detectable levels of transcript expression when subsequently profiled by RNA-seq [8]. Furthermore, in the majority of cases where tumour RNA was not also preserved along with the tumour DNA it can be extremely problematic to prove expression. However, detecting tumour genes using paired-end RNA-seq [5] not only identifies fusions but simultaneously provides quantification of their expression level. RNA-seq-based fusion gene detection therefore provides an additional means to filter for fusions more likely to be functionally relevant. Here, we have used RNA-seq-based fusion gene detection to identify gene fusions with putative functional relevance for neuroblastoma, a paediatric solid tumour with a lack of conventional somatic mutations [9-11]. This lack of recurrent somatic

mutations has hampered the development of targeted therapeutic approaches for neuroblastoma. Therefore, the identification of functionally relevant fusion genes may provide effective therapeutic targets to improve patient outcome.

Neuroblastoma arises from an embryonal tissue, the neural crest, due to improper terminal differentiation of neural crest derived stem cells [12-18], and is responsible for 15% of all childhood cancer deaths [19]. There is a relative paucity of recurrent activating somatic point mutations or gene fusions in neuroblastoma [9-11, 20]. However, this lack of fusion genes may be due to limited investigation rather than fusions being truly absent, especially given that fusions are an underappreciated class of mutations in solid tumours [5]. Indeed, given the paucity of recurrent somatic coding mutations in neuroblastoma [9] it is quite likely that fusion events have played a hitherto underappreciated role in contributing to tumourigenicity in this malignancy. We detected the novel fusion of the VANGL2 and ITLN1 genes in the neuroblastoma cell line IMR32 by applying FusionHunter [21] to our paired-end transcriptome sequencing. Both genes sit on chromosome 1, within 1q23 (human genome build: GRCh38/hg38). Chromosome 1 frequently harbours chromosomal abnormalities in neuroblastoma; for example, 70% of cases contain structural rearrangement of chromosome 1p [22]. Chromosome 1q gain occurs commonly in cancers (generally 1q23-1q32 region) and is more frequent in recurrent tumours, possibly associated with tumour progression [23, 24]. Specifically in neuroblastoma, 1q21-1q25 gain has been associated with progressive disease [23, 25].

VANGL2 (Van Gogh-Like Planar Cell Polarity Protein 2) encodes a membrane protein involved in the regulation of planar cell polarity [26] and is conserved among species from flies to mammals [27]. In vertebrates, Planar Cell Polarity genes play a role in embryonic development during gastrulation and neurulation, with VANGL2 itself being involved in neural tube closure [28, 29] and axonal guidance [30]. Studies have shown that VANGL2 is strongly expressed in the developing nervous system of mice [31], but also in adult rat neurons [32]. In mice and humans there are two VANGL-family members, VANGL1 and VANGL2, with about 70% amino-acid sequence identity, which have differing expression patterns [31, 33]. VANGL genes are increasingly being recognised for their involvement in a number of cancers [34-37], including the paediatric solid tumour neuroblastoma [38, 39]. VANGL2 is a key component of the Wnt/planar cell polarity pathway, as well as being associated with the canonical Wnt/β-catenin signalling pathway [36, 40], and its expression is associated with less differentiated cell types [38]. Both the Wnt/β-catenin signalling pathway

and the Wnt/planar cell polarity pathway are important regulators of neuroblastoma cell behaviour and patient outcome [38, 41-44]. A VANGL2-PDE4DIP fusion gene has previously been identified in adenocarcinoma [3] (Mitelman Database of Chromosome Aberrations and Gene Fusions in Cancer [2017], https://cgap.nci.nih.gov/Chromosomes/Mitelman).

ITLN1 (Intelectin-1) is usually expressed in the small intestine and the colon, where it is secreted from goblet cells into the mucus [45]. It can bind to specific structures on the surface of bacteria and might play a role in immune defence [45]. Upon infection or inflammation, an increase in the expression of ITLN1 mRNA can be observed in the intestine [46, 47] and in the bronchi of the lungs [48]. ITLN1 has been shown to be overexpressed and secreted from human malignant pleural mesothelioma [49, 50], and also in the majority of human gastric cancer tissues [51]. For the latter, there is a positive correlation between ITLN1 expression in gastric cancer and patient survival [51]. Additionally, *in vitro* transfection of the ITLN1 gene into gastric cancer cells [51] and prostate cancer cells [52] has led to attenuated proliferation and decreased *in vitro* cell viability, which indicates a tumour suppressor function for ITLN1 in those cells. Recently, ITLN1 has been shown to have a functional role in neuroblastoma, where its ectopic expression suppressed the growth, invasion and metastasis of neuroblastoma cells *in vitro* and *in vivo* [53]. Conversely, knockdown of ITLN1 promoted the growth, invasion, and metastasis of neuroblastoma cells [53].

Our findings reveal that neuroblastoma cell lines can harbour previously unidentified fusion genes and that the components of the VANGL2-ITLN1 fusion are associated with patient outcome. Importantly, our results highlight the need for comprehensive fusion gene screening in neuroblastoma tumour samples. Such analysis would be extremely timely given the advent of the precision medicine-era [54-56] and the associated dramatic increase in the number of tumours being transcriptomically sequenced.

Results

Identification of a VANGL2-ITLN1 fusion gene in IMR32 cells

Fusion genes play an increasingly well-recognised role in numerous tumour types [2-4]. We therefore mined paired-end RNA-seq data from five neuroblastoma cell lines (IMR32, SY5Y, Kelly, KCN and KCNR) for the presence of novel gene fusions, using FusionHunter [21]. We had previously generated this transcriptomic dataset to determine the MYCN signalling network functionally responsible for driving poor-outcome neuroblastoma [13, 43, 57-59],

and as such the cell lines cover a range of MYCN expression and amplification statuses [57, 58]. The FusionHunter analysis revealed the existence of a VANGL2-ITLN1 fusion gene in the MYCN amplified IMR32 cell line (Fig. 1A). The IMR32 cell line was derived from a metastatic neuroblastoma tumour and expresses high levels of MYCN [57, 58, 60]. The VANGL2-ITLN1 fusion gene was not detected in the other four cell lines, being unique to IMR32 cells. The fusion gene transcript comprises part of the 5' untranslated region (UTR) of the VANGL2 gene, and the complete and intact open reading frame (ORF) and 3' UTR of ITLN1 (Table 1, Fig. 1A).

Table 1. Sequence of the VANGL2-ITLN1 fusion gene mRNA transcript. The VANGL2 5' UTR is shaded in grey. Start and stop codons of the ITLN1 ORF are shaded in green.

VANGL2-ITLN1 fusion mRNA sequence

```
   1 GGCTCCCGAT CTGATTCCTG ATCCTTGATT CCTTGATCCT TGGTCCCGCC
  51 ATGGGAGCCT GAGCGCCCCC TATTCCCCCC TGGCCCCCAG CCCCCGGGGC
 101 CTTGAGGGGG AAGAGGCAGC GGTCTGGGAC GGAGCAGGGG GTGACCAGAC
 151 TCAAGAACCC CCCCCTCAAC ATCCCCCATC GCGCGCGCTG CCTGTCCAGG
 201 AGCGCCGAGT TCGGAGCGAC CCGGAGCGCT GCGGATACAA AGGCGACGGG
 251 CCGAGCGGGG CGCCCGCGGA GCCCACCCGG CAGTTCGCAG CGGCGGATTA
 301 CAATGAACCA ACTCAGCTTC CTGCTGTTTC TCATAGCGAC CACCAGAGGA
 351 TGGAGTACAG ATGAGGCTAA TACTTACTTC AAGGAATGGA CCTGTTCTTC
 401 GTCTCCATCT CTGCCCAGAA GCTGCAAGGA AATCAAAGAC GAATGTCCTA
 451 GTGCATTTGA TGGCCTGTAT TTTCTCCGCA CTGAGAATGG TGTTATCTAC
 501 CAGACCTTCT GTGACATGAC CTCTGGGGGT GGCGGCTGGA CCCTGGTGGC
 551 CAGCGTGCAC GAGAATGACA TGCGTGGGAA GTGCACGGTG GGCGATCGCT
 601 GGTCCAGTCA GCAGGGCAGC AAAGCAGTCT ACCCAGAGGG GGACGGCAAC
 651 TGGGCCAACT ACAACACCTT TGGATCTGCA GAGGCGGCCA CGAGCGATGA
 701 CTACAAGAAC CCTGGCTACT ACGACATCCA GGCCAAGGAC CTGGGCATCT
 751 GGCACGTGCC CAATAAGTCC CCCATGCAGC ACTGGAGAAA CAGCTCCCTG
 801 CTGAGGTACC GCACGGACAC TGGCTTCCTC CAGACACTGG GACATAATCT
 851 GTTTGGCATC TACCAGAAAT ATCCAGTGAA ATATGGAGAA GGAAAGTGTT
 901 GGACTGACAA CGGCCCGGTG ATCCCTGTGG TCTATGATTT TGGCGACGCC
 951 CAGAAAACAG CATCTTATTA CTCACCCTAT GGCCAGCGGG AATTCACTGC
1001 GGGATTTGTT CAGTTCAGGG TATTTAATAA CGAGAGAGCA GCCAACGCCT
1051 TGTGTGCTGG AATGAGGGTC ACCGGATGTA ACACTGAGCA CCACTGCATT
1101 GGTGGAGGAG GATACTTTCC AGAGGCCAGT CCCCAGCAGT GTGGAGATTT
1151 TTCTGGTTTT GATTGGAGTG GATATGGAAC TCATGTTGGT TACAGCAGCA
1201 GCCGTGAGAT AACTGAGGCA GCTGTGCTTC TATTCTATCG TTGAGAGTTT
1251 TGTGGGAGGG AACCCAGACC TCTCCTCCCA ACCATGAGAT CCCAAGGATG
1301 GAGAACAACT TACCCAGTAG CTAGAATGTT AATGGCAGAA GAGAAAACAA
1351 TAAATCATAT TGACTCAAAA AAAAAAAAAA AAAAAAAAAA AAAAA
```

To ensure that the detection of the fusion gene was not due to a sequencing or computational artefact we verified the presence of the VANGL2-ITLN1 fusion by conventional PCR and RT-qPCR using primers that were designed based on the fusion transcript sequence obtained from the RNA-seq data (Table 2). The full VANGL2-ITLN1 fusion transcript was amplified via conventional PCR and Sanger sequenced. Using qPCR we confirmed that the fusion gene

was only present in IMR32 cells, and not expressed in the other four cell lines (SY5Y, Kelly, KCN and KCNR).

Table 2. ITLN1 and VANGL2 primer sequences used for RT-qPCR and conventional PCR.

Primers list	Primer sequence	Product size
For detecting fusion expression:		
VANGL2 qPCR Fwd	GGGGTGACCAGACTCAAGAA	187bp
ITLN1 qPCR Rev	GCAGGAAGCTGAGTTGGTTC	
For detecting wild type expression:		
ITLN1 w.t. qFwd1	AGCGTTTTTGGAGAAAGCTG	135bp
ITLN1 qPCR Rev	As above	
VANGL2 w.t. qFwd1	CTCGGAGAGGAAAACAGCAC	192bp
VANGL2 w.t. qRev1	CAGCCGCTTAATGTGAGTGA	
For amplifying full fusion transcript:		
VANGL2 start Fwd	GGCTCCCGATCTGATTCC	1,369bp
ITLN1 end Rev	TTTGAGTCAATATGATTTATTGTTTTC	
For assessing background level of plasmid		
Plasmid Backbone qPCR Fwd	CAACCCGGTAAGACACGACT	76bp
Plasmid Backbone qPCR Rev	GCCTACATACCTCGCTCTGC	

The expression levels of the two fusion gene components were then examined in our neuroblastoma cell line RNA-seq data (Fig. 1B). VANGL2 was widely expressed across all five neuroblastoma cell lines, although IMR32, the cell line harbouring the VANGL2-ITLN1 fusion gene, had over double the level of VANGL2 expression seen in any other cell line. Conversely, ITLN1 expression was practically silenced in the other four neuroblastoma cell lines. We postulated that this ITLN1 expression in IMR32 was due to the fusion event, with the ITLN1 transcript's expression being driven by the ectopic upstream VANGL2 promoter. To assess the veracity of this assumption, qPCR primer sets capable of differentiating between VANGL2-ITLN1 fusion transcripts and wild type ITLN1 and wild type VANGL2 transcripts were designed (Table 2) and qPCR performed using cDNA generated from IMR32 cells (Fig. 1C). This confirmed that wild type VANGL2 transcripts are abundant in IMR32 cells, and revealed that wild type ITLN1 expression was practically silenced.

Interestingly, the expression of genes immediately upstream of VANGL2 (UCSC genome browser [61], human genome build: hg38) were elevated in IMR32 cells also, suggesting the

possibility of a larger mutational event (Fig. 1D, Table S1), likely due to a 1q21-1q25 gain known to occur in some neuroblastoma tumours [23, 25]. The VANGL2 and ITLN1 genes sit relatively close together on chromosome 1, being separated by only nine genes with the end of VANGL2 and the beginning of the ITLN1 gene being 447.9kb apart (Fig. 1D, UCSC genome browser [61], human genome build: hg38). Interestingly, the expression of the gene immediately upstream of VANGL2, NHLH1, was also highly elevated in IMR32 cells compared with the other four neuroblastoma cell lines (Fig. 1D and Table S1). Expression of NHLH1, a neurogenesis-related gene [62], has previously been linked with neuroblastoma [63, 64] with our results suggesting that NHLH1 expression may be altered by the same chromosomal translocation event responsible for generating the VANGL2-ITLN1 fusion.

ITLN1 and VANGL2 tumour expression levels are predictive of patient outcome

Having confirmed the expression of the fusion transcript in IMR32 cells we next determined if the results obtained from the cell line were relevant to neuroblastoma tumour biology. We examined whether there was any correlation between the two components of the fusion gene and neuroblastoma patient outcome in a large neuroblastoma tumour dataset (SEQC [65] with 498 tumours), using the R2: Genomics Analysis and Visualization Platform (http://r2.amc.nl). VANGL2 and ITLN1 mRNA expression levels were each prognostic of patient survival (Fig. 2A), with VANGL2 showing the strongest predictive power. Low VANGL2 expression was associated with worse outcome, which is interesting given that the VANGL2-ITLN1 fusion event in IMR32 results in a fusion product with no VANGL2 ORF/transcript. However, it should be noted that IMR32 cells do retain a functionally transcribed copy of VANGL2 (Fig. 1B, C), suggesting the fusion gene was generated by a trisomy event as is known to occur in that 1q region [23]. Interestingly, high ITLN1 expression was associated with worse outcome. When ITLN1 expression in these tumours was compared with neuroblastoma risk stage there was a significant difference between the stages (ANOVA, *p*-value = 9.4E-03), with higher expression levels tending towards higher classification stage (Fig. 3A). However, interestingly, stage 4S also tended towards higher expression of ITLN1. Despite having disseminated tumours, stage 4S patients have a good prognosis (due to phenomena such as spontaneous regression). Conversely, regular stage 4 patients have the lowest survival rate of all stages.

Given this stage-specific difference in ITLN1 expression, we next examined ITLN1's ability to predict survival probability in each tumour stage. Consistently, in each stage (including

4S) those tumours with higher ITLN1 expression showed a lower survival rate (Fig. 3B). We next examined whether there was any difference in ITLN1's ability to predict survivorship in MYCN amplified and MYCN non-amplified tumours. MYCN amplification status is the strongest single genetic marker prognostic for neuroblastoma outcome [66]. Once again in both groups, even when accounting for MYCN, the ITLN1 expression level was able to add additional predictive power to patient survival, with high ITLN1 expression being predictive of worse outcome in both MYCN status cohorts (Fig. 3C). Although it should be noted that while this difference was statistically significant in the non-amplified MYCN cohort (*p*-value = 2.9E-03), in the MYCN amplified cohort this trend was just shy of statistical significance (*p*-value = 0.054) due to the smaller sample size, and low overall survival rate. No patient with MYCN amplification and high ITLN1 expression survived beyond 36 months.

Other cancer cell lines and tumour samples harbour additional VANGL2 and ITLN1 mutations

Given that low levels of ITLN1 expression are associated with better patient outcome, we next examined two wider neuroblastoma cell line panels to assess the mutation and expression status of the fusion gene components. We mined a recent RNA-seq database of a 39 neuroblastoma cell line panel [67] and the catalogue of somatic mutations in cancer (COSMIC) (http://cancer.sanger.ac.uk/cosmic, COSMIC v81) database [68].

The low levels of ITLN1 expression in the neuroblastoma cell lines that we profiled which lacked the fusion gene (KCN, KCNR, Kelly and SY5Y) were consistent with ITLN1 expression across the 39 neuroblastoma cell lines profiled by RNA-seq by Harenza *et al.* [67] (Fig. 4A). ITLN1 expression was also extremely low in RPE1 cells (a retinal pigment epithelial cell line) and human foetal brain tissue, which was also profiled in the Harenza *et al.* study [67] (Fig. 4A). ITLN1 was practically silenced across the 39 neuroblastoma cell lines, with only four of them showing ITLN1 expression. Similar to our five cell line panel, almost all of the neuroblastoma cell lines had high levels of VANGL2 expression (Fig. 4A).

We also utilised the catalogue of somatic mutations in cancer (COSMIC) (http://cancer.sanger.ac.uk/cosmic, COSMIC v81)[68] database to further examine the fusion component genes in neuroblastoma cells and cancer more generally. Two of 34 neuroblastoma cell lines in the COSMIC database harboured ITLN1 over- or under-expression, while almost half of these 34 cell lines showed VANGL2 overexpression (Table 3). While a VANGL2-ITLN1 fusion gene has not previously been reported in the COSMIC

database, both of these genes do have a number of mutations and altered expression patterns in both cancer tissue and cell line samples (Table 4), further supporting their potential relevance to oncogenic processes. Interestingly, in tumour samples with altered VANGL2 or ITLN1 expression, both genes were predominantly overexpressed, rather than underexpressed, indicating that excess transcription of these genes (as seen in the IMR32 cell line, largely due to the fusion gene) is associated with tumours.

Table 3. Expression status of 34 neuroblastoma cell lines present in the COSMIC database.

Neuroblastoma cell lines in COSMIC database with over/under expression of VANGL2 or ITLN1	Expression status	Exp. level z score	Average ploidy
ITLN1:			
CHP-212	Under	-2.28	1.98
NB7	Over	2.40	3.04
VANGL2:			
BE2-M17	Over	3.39	1.84
CHP-126	Over	2.83	2.01
CHP-134	Over	2.51	1.97
GOTO	Over	3.54	2.02
IMR-5	Over	4.41	2.05
KELLY	Over	2.11	1.99
KP-N-YN	Over	2.81	1.93
MHH-NB-11	Over	2.45	2.40
NB(TU)1-10	Over	2.48	3.00
NB1	Over	2.32	1.94
NB10	Over	2.24	3.39
NB17	Over	2.05	2.97
SIMA	Over	2.25	3.86
SK-N-DZ	Over	2.10	3.90
TGW	Over	2.02	3.17

Table 4. ITLN1 and VANGL2 mutation and expression status in COSMIC database tumour and cell line samples.

	Tested samples	Curated fusions	Mutated	Over expressed	Under expressed
ITLN1:					
Tumour samples	29,379	0	126	276	0
Cancer cell lines	1,020	0	28	23	27
NB cell lines only	34	0	2	1	1
VANGL2:					
Tumour samples	29,379	0	178	895	13
Cancer cell lines	1,020	0	51	57	20
NB cell lines only	34	0	1	15	0

We further analysed how the expression levels of the fusion gene components in neuroblastoma compared with levels in other healthy and malignant tissues using the *In Silico* Transcriptomics (IST) Online database (http://ist.medisapiens.com/, version 2.1.3) which

contains human transcriptomics data for 3,082 healthy tissue samples, 15,392 malignant tissue samples and 1,590 other disease samples. In line with the other datasets, VANGL2 expression was highly elevated in neuroblastoma tissue compared with healthy tissue types, with only prostate, penis and vagina/vulva tissues reaching VANGL2 expression levels similar to that of neuroblastoma (Fig. 4B). Furthermore, the neuroblastoma cohort expressed higher VANGL2 levels than the majority of other malignancies, although generally VANGL2 expression was elevated in across malignancies compared with healthy tissues (Fig. 4B). Interestingly, melanoma samples had a similarly high level of VANGL2 mRNA to that seen in neuroblastoma. Both melanocyte and neuroblast cells share a common tissue of origin, the embryonal tissue the neural crest whose induction and migration is associated with canonical and Wnt/PCP signalling [43, 69-71]. The IST Online database once again confirmed that endogenous ITLN1 expression was very low in neuroblastoma samples (Fig. 4B). The IST Online database's cell line panel also confirmed that VANGL2 tends to be more highly expressed than ITLN1 across the majority of cell types (Fig. 4C).

We next examined patient outcome and expression patterns of WNT5A (Figs 4D, S1A). WNT5A is the main Wnt ligand associated with the Wnt/PCP pathway of which VANGL2 is a downstream component [38, 43, 72, 73]. Mirroring VANGL2, patients with low WNT5A had worse outcomes. However, a larger cohort of patients harboured low VANGL2 expressing tumours than WNT5A, indicating that alterations/mutations of the PCP pathway in neuroblastoma more commonly occur downstream of the Wnt ligand with VANGL2 expression levels providing a more broadly informative readout of patient outcome. The fact that more downstream alterations to the Wnt/PCP pathway are a more common feature is supported by recent findings that Wnt-related genes, including VANGL1, are recurrently mutated in relapsed neuroblastoma [39, 74, 75].

VANGL2-ITLN1 fusion expression can be transcriptionally regulated by lithium chloride

Having confirmed that altered expression and mutations in the component genes of the VANGL2-ITLN1 fusion are present in other neuroblastoma and cancer cell lines, we next examined whether the expression of the fusion gene was under transcriptional control of the VANGL2 promoter. VANGL2 is regulated by canonical and non-canonical Wnt signalling. Additionally, VANGL2 interacts at the protein level with Wnt genes (Fig. S1B), being a key Wnt/planar cell polarity pathway component [36, 40, 76]. When IMR32 cells were treated

with lithium chloride (LiCl) (an inhibitor of GSK3β that activates Wnt/β-catenin pathway activity [57]), both VANGL2 and ITLN1 expression increased by a similar fold change (Fig. 5A), suggesting that the fusion gene in IMR32 cells is indeed under similar translational control as wild type VANGL2, i.e. the VANGL2 upstream promoter is also likely fused to and regulating the expression of the ITLN1 gene. We used our qPCR assays to examine the specific lithium-induced changes in expression for the VANGL2-ITLN1 fusion transcript and the wild type VANGL2 and ITLN1 transcripts. This revealed that all three transcripts were upregulated by LiCl, and that the change in fusion gene expression most closely resembled that of wildtype VANGL2 (Fig. 5A).

VANGL2 and ITLN1 interact with the MYCN oncogenic network

In line with VANGL2 mutations predominantly occurring in relapsed rather than primary neuroblastoma, the fusion gene does not appear to be involved in the initial stages of oncogenic transformation. Overexpression of the fusion gene in a NIH-3T3 mouse fibroblasts focus formation assay by transfection with a pcDNA3 plasmid containing the full length fusion transcript did not increase foci formation, despite the transcript being expressed (Fig. S1C, D). The effect of the fusion gene components on neuroblastoma patient outcome (Figs 2A, 3A-C) is likely due to these genes modulating post-initiation events such as neuroblastoma progression, resistance to therapy or metastasis through interaction with other neuroblastoma genetic drivers. Therefore, we next examined known regulatory network interactions involving the fusion gene components.

Amplification of the MYCN oncogene is the strongest single gene prognostic factor for neuroblastoma patient outcome (Fig. 3C), with MYCN being amplified in 20% of neuroblastoma tumours [17, 66, 77-79]. IMR32 cells are MYCN amplified and express high levels of MYCN mRNA and protein [57, 58]. For this reason we examined whether any links exist between MYCN and the two component genes of the VANGL2-ITLN1 fusion. We used the Genome-scale Integrated Analysis of Gene Networks in Tissues (GIANT, http://giant.princeton.edu/) programme [80] to examine whether interactions exist between MYCN and the two components of the fusion gene. MYCN had direct links to both VANGL2 and ITLN1, as well as all three genes being part of an interconnected network (Fig. 5B), suggesting that these genes (and therefore potentially the fusion gene) may cooperate with the MYCN oncogene in playing a role in poor outcome neuroblastoma. Interestingly, ALK was also a direct edge of ITLN1. ALK is another key neuroblastoma driver gene

recurrently mutated in tumours and can drive poor outcome, both in cooperation with and independently of the MYCN oncogene [66, 81].

Finally, we mined our extensive MYCN overexpression omics data [58] to identify any points of interaction between the fusion component genes and MYCN (Figs 5C, S2A-C). This analysis showed that a putative protein-protein interaction exists between MYCN and ITLN proteins (MYCN mass spec. coIP, Fig. S2A). It also showed that MYCN protein directly binds to the DNA of the VANGL1 and VANGL2 genes (MYCN ChIP-seq, Table S2) and that MYCN overexpression exerts a modest repressive effect on VANGL2 transcription (MYCN overexpression 4sU-seq, Fig. S2B). Taken together these findings reveal cross-talk between the MYCN oncogene and the two component genes of the VANGL2-ITLN1 fusion, and suggest that the fusion gene may play a functional role contributing to poor outcome neuroblastoma.

Discussion

This study has demonstrated the potential for previously undiscovered fusion genes to exist in neuroblastoma, even being harboured in a widely studied neuroblastoma cell line, IMR32. We confirmed the fusion of the VANGL2 and ITLN1 genes in IMR32 cells, and that the fusion was not present in other neuroblastoma cell lines tested (Kelly, KCN, KCNR and SY5Y). The fusion essentially drives the overexpression of the ITLN1 gene, linking it to VANGL2's upstream transcriptional regulatory apparatus, and removing the ITLN1 5' UTR from the transcript. Although the fusion event could have conceivably resulted in reduced expression of VANGL2, wild type VANGL2 expression remains high in IMR32. This suggests that the fusion was generated by a trisomy event known to occur at that chromosomal location in a number of malignancies [23]. At the very least the presence of the fusion gene may have implications for studies on the widely utilised IMR32 neuroblastoma cell line, which is used not only as a neuroblastoma model but also as a neurological model for a range of conditions, e.g. Alzheimer's disease [82]. The results of such studies may need to be reinterpreted in light of the presence of this novel fusion gene, particularly for those studies directly investigating VANGL2, ITLN1 or their immediate networks and interactors [38]. However, the fusion may have wider relevance given the statistically significant associations between the fusion gene components and neuroblastoma patient outcome, the known chromosomal rearrangements at 1q [23, 25], the VANGL coding mutations recently identified in relapsed neuroblastoma tumours [39], the historical lack of effort to

systematically identify neuroblastoma fusions, and the fusion components being MYCN-related genes.

There is a growing appreciation of the role of VANGL2 and indeed the Wnt pathways themselves in neuroblastoma biology, including their contribution to the maintenance of more stem-like states associated with worse outcome [13, 38, 42-44]. Furthermore, mutations in Wnt component genes have recently been identified by deep sequencing of recurrent/relapsed neuroblastoma tumours [39, 74, 75]. Our analysis adds fusion events to the mechanisms by which VANGL genes are mutated in neuroblastoma. Furthermore, VANGL2 sits adjacent to NHLH1 on chromosome 1, in a chromosomal region frequently containing structural rearrangements in neuroblastoma [22, 23, 25]. We show that the VANGL1 and VANGL2 genes are bound by MYCN protein (MYCN ChIP-seq), a gene known to drive chromosomal instability. Our analysis highlights the strong correlation between VANGL2 expression and neuroblastoma patient outcome (Fig. 2A) and the gene's elevated expression in neuroblastoma cell lines, mirroring the high expression observed in human foetal brain tissue (Fig. 3A). We also demonstrated that VANGL2's 5' UTR region likely conferred its Wnt transcriptional responsiveness upon the VANGL2-ITLN1 fusion.

Recently it has been shown that ITLN1 attenuated the growth and metastasis of SY5Y-derived tumours *in vivo*. When SY5Y cells with ITLN1 overexpression were injected into nude mice the overall tumour weight and the occurrence of lung metastasis were reduced compared with those of wild-type SY5Y-derived tumours [53]. Conversely, ITLN1 knock down increased the weight of SY5Y-derived tumours and the occurrence of lung metastasis [53]. These authors also claimed that high ITLN1 expression was associated with good outcome in neuroblastoma patients, a finding in direct contrast with our analysis (Fig. 2A). Crucially, however, Li *et al.* based this finding on a small patient cohort (also obtained from the R2 microarray analysis and visualization platform) consisting of only 57 neuroblastoma patients, a mere eight of which exhibited high ITLN1 expression. Our analysis from a cohort of 498 neuroblastoma patients reveals that high ITLN1 expression in fact correlates with poor outcome. Furthermore, this correlation holds true across all tumour stages and independently of MYCN amplification status (Fig. 3). However, our analysis also suggests that the effect of elevated ITLN1 expression may be exacerbated depending on the genetic background of the tumour, as, strikingly, no patients with MYCN amplification and high ITLN1 expression survived beyond 36 months post diagnosis (Fig. 3C). Therefore, the genetic background of a tumour, particularly its MYCN amplification status, may account for the discrepancy in the

effects of ITLN1. We show here that ITLN1 is part of a MYCN regulatory network potentially even having direct protein-protein interactions with MYCN. In this light it should be noted that Li *et al.*'s *in vivo* assay used SY5Y cells which are not a MYCN-amplified cell line, and express minimal levels of MYCN [58]. ITLN1's role in neuroblastoma could be further complicated depending on whether a tumour harbours an activating ITLN1 fusion. The rate of ITLN1 fusions in neuroblastoma tumours is not currently known, and we cannot precisely segregate patient outcome by presence or absence of fusions using the available microarray cohorts. However, we do know that SY5Y cells neither harbour the VANGL2-ITLN1 fusion transcript (qPCR, data not shown, and FusionHunter analysis) nor express ITLN1 (Fig. 1B). Therefore, the beneficial phenotypes observed by Li *et al.* occurred in a background lacking MYCN amplification or VANGL2-ITLN1 fusion and it would be extremely interesting to determine whether repeating the assay with cell lines representing more high-risk neuroblastoma (e.g. IMR32 cells) would produce similar phenotypes. Our findings suggest an association between elevated ITLN1 expression, genetic-background effects on ITLN1 function and of a putative role in more advanced neuroblastoma, and are supported by the literature related to chromosome 1q gain. Chromosome 1q gain, the region including both the VANGL2-ITLN1 fusion component genes, occurs in a number of cancers including neuroblastoma, and is more frequent in recurrent tumours, having been linked to tumour progression [23-25]. We recommend that in-depth functional studies be conducted to comprehensively determine the role of ITLN1 and VANGL2 in neuroblastoma outcome, and that such studies also consider the possible effects of the VANGL2-ITLN1 fusion gene.

Although segmental chromosomal aberrations are common in neuroblastoma, translocation events that create fusion oncogenes are rarely seen in neuroblastomas at diagnosis, but do occur more frequently in relapsed disease after exposure to intensive DNA damaging chemotherapeutic agents [11]. Prior to the broad adoption of deep sequencing technologies in neuroblastoma research, Santo *et al*. (2012) [83] identified the transcriptional activation of the normally silenced FOXR1, in the 11q23 region, by a deletion-fusion in a number of neuroblastoma tumours. Fusion transcripts involving the ALK, NBAS, PTPRD, ARHGEF33 and ODZ4 genes have also previously been identified [8]. However, that study only profiled two neuroblastoma tumours. Fusion analysis should be more generally applied to neuroblastoma tumours and indeed other malignancies and disease types to fully utilise the rich information currently being generated by deep sequencing technologies, as precision medicine initiatives result in an ever increasing cohort of genomically and transcriptomically

profiled tumours [54-56]. Indeed, eight putative fusion genes were recently detected in a panel of 151 neuroblastoma tumour samples genomically profiled by next-generation sequencing [75]. However, the authors did not confirm whether these putative fusions were expressed, again highlighting the inherent advantage of using RNA sequencing-based approaches for novel fusion gene detection enabling simultaneous transcriptional validation and quantification.

The novel VANGL2-ITLN1 gene fusion identified here has the potential to be involved in driving neuroblastoma tumorigenesis and poor patient outcomes owing to the association of the fusion with regulatory networks such as MYCN, ALK and the Wnt/PCP pathway, which are key regulators of neuroblastoma outcome [11, 13, 15, 38, 58, 72, 84-86]. Given the variety of developmental processes with which the fusion component genes are associated, mutations in these genes may have implications beyond oncology, particularly for neuronal-related diseases. Our identification of the VANGL2-ITLN1 fusion highlights the underappreciation of the potential contribution of gene fusions to malignancies, being present even in a model system previously considered to be well characterised. Fusion gene analysis should become a standard test in human oncology and other non-communicable diseases over the coming decades as genomic-era medicine continues to be more widely implemented in the clinic.

Materials and Methods

Fusion gene detection using paired-end RNA sequencing

We mined our previously generated neuroblastoma paired-end RNA-seq data [57, 58] for fusion genes. For a description of how the RNA-seq experiments were conducted and our initial bioinformatics analysis, please see the following references: [57, 58, 87]. Five neuroblastoma cell lines (IMR32, SY5Y, Kelly, KCN and KCNR) were examined for the presence of novel gene fusions using FusionHunter [21] with stringent parameters. Fusion genes were called only if a minimum of two mate pairs mapping at the two different genomic locations and at least a single read mapped across the junction. Single read mapping across junctions was used to determine the exact breakpoint.

ArrayExpress (http://www.ebi.ac.uk/arrayexpress) accession numbers or RNA-seq datasets used in this study were: E-MTAB-1684, E-MTAB-2690, E-MTAB-2691, E-MTAB-2787, E-MTAB-4100 and E-MTAB-2689. The VANGL2-ITLN1 fusion transcript sequence was

deposited in NCBI's GenBank (https://www.ncbi.nlm.nih.gov/genbank/, accession number pending).

Cell lines and culture conditions

Cell lines were cultured as previously described [57]. Briefly, Kelly, SMS-KCN, SMS-KCNR and IMR32 cells were cultured in RPMI-1640 media (Invitrogen) supplemented with 2mM L-glutamine, 10% fetal bovine serum (FBS) and 1% penicillin/streptomycin in Nunc cell culture flasks (Thermo Scientific) and maintained at 37°C in a humidified atmosphere. The culture medium for SH-SY5Y-MYCN cells (inducible expression system SH-SY5Y/6TR(EU)/pTrex-Dest-30/MYCN [88]) additionally contained G418 and Blasticidin. NIH-3T3 mouse fibroblast cells were cultured in DMEM (Invitrogen) supplemented with 2mM L-glutamine, 10% FBS and 1% penicillin/streptomycin. Upon transfection, NIH-3T3 cells were cultivated in DMEM media supplemented with 10% DBS (Donor Bovine Serum, Invitrogen) until they reached full confluency. The cells were harvested using Versene (1mM EDTA in 1 x PBS) for the neuroblastoma cell lines or 0.25% Trypsin-EDTA (Gibco) for NIH-3T3 cells.

RNA extraction and reverse transcription

RNA was isolated from cell lines using the RNeasy Mini Kit (Qiagen) according to the manufacturer's instructions. RNA concentration was measured using the NanoDrop 2000 (Thermo Scientific). For generating cDNA for standard PCR, 5 µg of total RNA were subjected to a DNA-removal step using the Dnase I Rnase-free Kit (Roche). Reverse transcription was performed using the High-Capacity cDNA Reverse Transcription Kit (Invitrogen). We used an equivalent of 1 µg of DNA-free RNA, and 1 µl oligo(dT)$_{12-18}$-primers (Invitrogen) to a final concentration of 25 ng/µl for the reverse transcription reaction. For qPCRs, cDNA was synthesised as previously described [57], using a QuantiTect Reverse Transcription Kit (Qiagen) including the gDNA removal with step.

Conventional PCR

Note that amplification of the full-length fusion transcript proved to be difficult. We tested several different polymerases according to the manufacturer's protocols: GoTaq DNA Polymerase (Promega), PfuUltra High-Fidelity DNA Polymerase (Agilent Technologies) and Platinum Taq DNA Polymerase (Life Technologies), with only Platinum Taq providing successful full-length amplification. Amplification of the full length VANGL2-ITLN1 fusion

gene was successful using the Platinum Taq polymerase (Life Technologies) at 55°C annealing temperature and 2mM $MgSO_4$ (PCR program: 95°C 2min, (95°C 15sec, 55°C 30sec, 68°C 3min) x 35, 68°C 4min). For primer sequences please see Table 2. The PCR product of approximately 1400bp was purified from an agarose gel using the QIAquick Gel Extraction Kit (Qiagen) and confirmed by Sanger sequencing (MWG Eurofins).

VANGL2-ITLN1 fusion gene plasmid construction

The full length fusion gene, obtained by PCR, was cloned into the pJET1.2/blunt cloning vector (CloneJET PCR Kit, Thermo Scientific) using the sticky end protocol according to the manufacturer's instructions. It was amplified by transformation into DH5α competent *E. coli* cells as follows: 3 µl of the ligated vector were added to 50 µl of competent bacteria, incubated on ice for 30 min and heat shocked at 42°C for 30 sec. For plasmid expression, 250 µl of SOC-medium (Invitrogen) were added to the cells and they were incubated for 1 h at 37°C and 800 rpm. 50 µl of the mixture was then plated on agar plates containing 100 µg/ml ampicillin. Positive cultures were selected by colony PCR and propagated in 3 ml LB-medium (100 µg/ml ampicillin) overnight. The plasmids were retrieved using a Plasmid Mini Kit (Qiagen) and correct insertion of the fusion gene was verified by Sanger sequencing (MWG Eurofins). The insert was then cut out of the cloneJET vector with the BglII restriction enzyme and purified on an agarose gel using the QIAquick Gel Extraction Kit (Qiagen). Since the insertion into the mammalian expression vector pcDNA3-Flag was required both in forward and reverse orientation (due to the open reading frames in the non-coding strand), both insert and pcDNA3-Flag (cut open with EcoRI) were blunted using the blunting enzyme from the Thermo Scientific CloneJET Kit before ligation. The ligation itself was then performed using an insert-to-vector ratio of 3:1 (69 ng : 90 ng = 0.075 mol : 0.025 mol) and 2 µl T4-Ligase (New England Biolabs) in a 20 µl reaction mixture. The mixture was incubated for 20 min at RT, before 3 µl were taken off diluted in 5 µl 1 x T4 reaction buffer and incubated for another 1 h at room temperature. All of the 8 µl reaction was subsequently used for transfection of DH5α cells as described above. Positive clones were identified by colony PCR, propagated and plasmids extracted, as above. The orientation of the insert was assessed by restriction digest with *Eco*RI and *Kpn*I and verified by sequencing (MWG Eurofins). Finally, one clone was selected for each of the forward and the reverse oriented insert and propagated in 50 ml LB medium (100 µg/ml ampicillin) for plasmid extraction (Qiagen, EndoFree Plasmid Maxi Kit).

Transfection into NIH 3T3 cells (Lipofectamine2000) / Focus formation assay

NIH-3T3 cells were cultivated in DMEM with 10% FCS, Penicillin / Streptomycin and 1 x Glutamine in a 175cm² flask until confluent. The cells were trypsinised and approximately 20,000 cells were seeded into 10 cm plates in 9 ml complete medium. The next day, the cells were transfected with pcDNA3 using Lipofectamine 2000 (Invitrogen) according to the manufacturer's instructions, and different amounts of plasmid DNA (1 µg, 2 µg or 4 µg per plate). Empty vector pcDNA3 was used as a negative control, and activated H-Ras12V as a positive control. For each 10 cm plate, 10 µl Lipofectamine was diluted in 240 µl serum-free medium and incubated for 5 min. Analogously, an appropriate amount of DNA (1 µg, 2 µg or 4 µg) was diluted in 250 µl serum-free medium and combined with the diluted Lipofectamine (total volume = 500 µl per 10 cm plate). The mixture was incubated for 20 min at RT before it was added to the cells. 6 h after transfection, the medium was removed, cells were washed with PBS and from that point on cultivated in DMEM supplemented with 10% donor bovine serum (DBS), Penicillin/Streptomycin, and 1x Glutamine. The cells were incubated at 37°C for 4 weeks (3 weeks for the H-Ras12V control cells), with the medium exchanged every 2-3 days. For analysis, the cells were washed with PBS, fixed in 100% methanol for 10 min and then stained with Giemsa solution (5% Giemsa stain (Sigma) in PBS) for 1 h. Subsequent destaining was done overnight using tap water. The plates were then dried and cell foci were imaged and counted manually.

qRT-PCR

RT-PCR (RT-qPCR) were performed as previously described [57]. For the sequences of primer pairs used please see Table 2. Additionally, TaqMan assays (Applied Biosystems) for the endogenous control genes used were RPLPO (4310879E) and ACTB (β-actin, 4326315E). TaqMan PCR Master Mix (Applied Bio Systems) was used for all TaqMan assays, while Power SYBR Green PCR Master Mix (Applied Biosystems) was used for all non-TaqMan assays. Biological duplicates were generated for all samples; technical replicates for every sample were also performed.

To verify the expression of forward and reverse insert of pcDNA3-transfected NIH-3T3 mouse fibroblasts, in addition to the VANGL2-ITLN1 fusion gene primers, and to subtract the background signal from contaminating plasmids that were carried over from the transfection, we used a set of pcDNA3 backbone primers (see Table 2).

MYCN overexpression datasets (ChIP-seq, transcriptomics and interaction proteomics)

In addition, to the RNA-seq data described above we examined fusion gene related data in a number of omic datasets (RNA-seq, MYCN ChIP-seq and MCYN mass spectrometry-based interaction proteomics) which we had previously generated. For methods related to the generation of these omics datasets please see the following publications: Duffy et al. 2014, Duffy *et al.* 2014, Duffy *et al.* 2015, Schwarzl *et al.* 2015, Duffy *et al.* 2016 and Duffy *et al.* 2017 [13, 43, 57, 58, 87].

Acknowledgements: Warmest thanks to Jenny Whilde, to the Conway Core Facilities staff (Alison Murphy, Karolina Jankowska, Catherine Moss) and the SBI support staff (Amaya Garcia Munoz and Ruth Pilkington). Warm thanks are also due to Frank Westermann, Johannes Schulte, Sven Lidner and Andrea Odersky for the generous gifting of cell lines. Funding was generously provided by the European Union Seventh Framework Programme (FP7/2007- 2013) ASSET project under grant agreement number FP7-HEALTH-2010-259348-2, Science Foundation Ireland (SFI) grant number 06/CE/B1129, and a Welsh Government Sêr Cymru II and the European Union's Horizon 2020 research and innovation programme under the Marie Skłodowska-Curie grant agreement No. 663830 -BU115.

References

1. Mitelman, F., B. Johansson, and F. Mertens, *The impact of translocations and gene fusions on cancer causation.* Nat Rev Cancer, 2007. **7**(4): p. 233-245.
2. Kumar-Sinha, C., S. Kalyana-Sundaram, and A.M. Chinnaiyan, *Landscape of gene fusions in epithelial cancers: seq and ye shall find.* Genome Medicine, 2015. **7**(1): p. 129.
3. Yoshihara, K., et al., *The landscape and therapeutic relevance of cancer-associated transcript fusions.* Oncogene, 2015. **34**.
4. Stransky, N., et al., *The landscape of kinase fusions in cancer.* Nat Commun, 2014. **5**.
5. Edgren, H., et al., *Identification of fusion genes in breast cancer by paired-end RNA-sequencing.* Genome Biology, 2011. **12**(1): p. R6.
6. Boer, J.M. and M.L. den Boer, *BCR-ABL1-like acute lymphoblastic leukaemia: From bench to bedside.* European Journal of Cancer, 2017. **82**: p. 203-218.
7. Erkizan, H.V., V.N. Uversky, and J.A. Toretsky, *Oncogenic partnerships: EWS-FLI1 protein interactions initiate key pathways of Ewing's sarcoma.* Clinical Cancer Research, 2010. **16**(16): p. 4077-4083.
8. Boeva, V., et al., *Breakpoint Features of Genomic Rearrangements in Neuroblastoma with Unbalanced Translocations and Chromothripsis.* PLOS ONE, 2013. **8**(8): p. e72182.
9. Pugh, T.J., et al., *The genetic landscape of high-risk neuroblastoma.* Nature Genetics, 2013. **45**(3): p. 279-284.
10. Sausen, M., et al., *Integrated genomic analyses identify ARID1A and ARID1B alterations in the childhood cancer neuroblastoma.* Nat Genet, 2013. **45**(1): p. 12-17.
11. Bosse, K.R. and J.M. Maris, *Advances in the translational genomics of neuroblastoma: From improving risk stratification and revealing novel biology to identifying actionable genomic alterations.* Cancer, 2016. **122**(1): p. 20-33.
12. Ross, R.A., et al., *Human neuroblastoma I-type cells are malignant neural crest stem cells.* Cell growth & differentiation: the molecular biology journal of the American Association for Cancer Research, 1995. **6**(4): p. 449-456.
13. Duffy, D.J., et al., *Retinoic acid and TGF-β signalling cooperate to overcome MYCN-induced retinoid resistance.* Genome Medicine, 2017. **9**(1): p. 15.

14. Tsokos, M., et al., *Differentiation of human neuroblastoma recapitulates neural crest development. Study of morphology, neurotransmitter enzymes, and extracellular matrix proteins.* The American Journal of Pathology, 1987. **128**(3): p. 484-496.
15. Schulte, J.H., et al., *MYCN and ALKF1174L are sufficient to drive neuroblastoma development from neural crest progenitor cells.* Oncogene, 2013. **32**(8): p. 1059-1065.
16. Olsen, R., et al., *MYCN induces neuroblastoma in primary neural crest cells.* Oncogene, 2017. **In press**.
17. Maris, J.M., *Recent Advances in Neuroblastoma.* New England Journal of Medicine, 2010. **362**(23): p. 2202-2211.
18. Tee, A., et al., *Neuroblastoma: A Malignancy Due to Cell Differentiation Block.* In Tech: Neuroblastoma - Present and Future, 2012: p. 79-84.
19. Maris, J.M., et al., *Neuroblastoma.* The Lancet, 2007. **369**(9579): p. 2106-2120.
20. Molenaar, J.J., et al., *Sequencing of neuroblastoma identifies chromothripsis and defects in neuritogenesis genes.* Nature, 2012. **483**(7391): p. 589-593.
21. Li, Y., et al., *FusionHunter: identifying fusion transcripts in cancer using paired-end RNA-seq.* Bioinformatics, 2011. **27**(12): p. 1708-1710.
22. Gilbert, F., et al., *Human neuroblastomas and abnormalities of chromosomes 1 and 17.* Cancer Res, 1984. **44**(11): p. 5444-9.
23. Puri, L. and J. Saba, *Getting a Clue from 1q: Gain of Chromosome 1q in Cancer.* Journal of Cancer Biology & Research, 2014. **2**(3).
24. Weith, A., et al., *Report of the second international workshop on human chromosome 1 mapping 1995.* Cytogenetics and Cell Genetics, 1996. **72**(2): p. 114.
25. Hirai, M., et al., *1q23 gain is associated with progressive neuroblastoma resistant to aggressive treatment.* Genes, Chromosomes and Cancer, 1999. **25**(3): p. 261-269.
26. Kibar, Z., et al., *Ltap, a mammalian homolog of Drosophila Strabismus/Van Gogh, is altered in the mouse neural tube mutant Loop-tail.* Nat Genet, 2001. **28**(3): p. 251-5.
27. Torban, E., C. Kor, and P. Gros, *Van Gogh-like2 (Strabismus) and its role in planar cell polarity and convergent extension in vertebrates.* Trends Genet, 2004. **20**(11): p. 570-7.
28. Torban, E., et al., *Tissue, cellular and sub-cellular localization of the Vangl2 protein during embryonic development: effect of the Lp mutation.* Gene Expr Patterns, 2007. **7**(3): p. 346-54.
29. Torban, E., et al., *Independent mutations in mouse Vangl2 that cause neural tube defects in looptail mice impair interaction with members of the Dishevelled family.* J Biol Chem, 2004. **279**(50): p. 52703-13.
30. Shafer, B., et al., *Vangl2 Promotes Wnt/Planar Cell Polarity-like Signaling by Antagonizing Dvl1-Mediated Feedback Inhibition in Growth Cone Guidance.* Developmental Cell, 2011. **20**(2): p. 177-191.
31. Tissir, F. and A.M. Goffinet, *Expression of planar cell polarity genes during development of the mouse CNS.* Eur J Neurosci, 2006. **23**(3): p. 597-607.
32. Yoshioka, T., et al., *Vangl2, the planar cell polarity protein, is complexed with postsynaptic density protein PSD-95 [corrected].* FEBS Lett, 2013. **587**(10): p. 1453-9.
33. Katoh, Y. and M. Katoh, *Comparative genomics on Vangl1 and Vangl2 genes.* Int J Oncol, 2005. **26**(5): p. 1435-40.
34. Hatakeyama, J., et al., *Vangl1 and Vangl2: planar cell polarity components with a developing role in cancer.* Endocrine-Related Cancer, 2014. **21**(5): p. R345-R356.
35. Puvirajesinghe, T.M., et al., *Identification of p62/SQSTM1 as a component of non-canonical Wnt VANGL2–JNK signalling in breast cancer.* 2016. **7**: p. 10318.
36. Katoh, M., *WNT/PCP signaling pathway and human cancer (review).* Oncology reports, 2005. **14**(6): p. 1583.
37. Daulat, A.M. and J.-P. Borg, *Wnt/Planar Cell Polarity Signaling: New Opportunities for Cancer Treatment.* Trends in Cancer, 2017. **3**(2): p. 113-125.
38. Dyberg, C., et al., *Planar cell polarity gene expression correlates with tumor cell viability and prognostic outcome in neuroblastoma.* BMC Cancer, 2016. **16**(1): p. 1-14.
39. Li, Y., et al., *Genomic analysis-integrated whole-exome sequencing of neuroblastomas identifies genetic mutations in axon guidance pathway.* Oncotarget, 2017. **8**(34): p. 56684-56697.
40. Katoh, M., *Strabismus (STB)/Vang-like (VANGL) gene family (Review).* International journal of molecular medicine, 2002. **10**: p. 11-16.
41. Szemes, M., et al., *Wnt Signalling Drives Context-Dependent Differentiation or Proliferation in Neuroblastoma.* Neoplasia, 2018. **20**(4): p. 335-350.
42. Becker, J. and J. Wilting, *WNT signaling, the development of the sympathoadrenal–paraganglionic system and neuroblastoma.* Cellular and Molecular Life Sciences, 2018. **75**(6): p. 1057–1070.
43. Duffy, D.J., et al., *Wnt signalling is a bi-directional vulnerability of cancer cells.* Oncotarget, 2016. **7**(37): p. 60310-60331.
44. Corda, G. and A. Sala, *Non-canonical WNT/PCP signalling in cancer: Fzd6 takes centre stage.* Oncogenesis, 2017. **6**: p. e364.
45. Tsuji, S., et al., *Human intelectin is a novel soluble lectin that recognizes galactofuranose in carbohydrate chains of bacterial cell wall.* J Biol Chem, 2001. **276**(26): p. 23456-63.
46. Datta, R., et al., *Identification of novel genes in intestinal tissue that are regulated after infection with an intestinal nematode parasite.* Infect Immun, 2005. **73**(7): p. 4025-33.

47. French, A.T., et al., *Up-regulation of intelectin in sheep after infection with Teladorsagia circumcincta.* Int J Parasitol, 2008. **38**(3-4): p. 467-75.
48. Kuperman, D.A., et al., *Dissecting asthma using focused transgenic modeling and functional genomics.* J Allergy Clin Immunol, 2005. **116**(2): p. 305-11.
49. Washimi, K., et al., *Specific expression of human intelectin-1 in malignant pleural mesothelioma and gastrointestinal goblet cells.* PLoS One, 2012. **7**(7): p. e39889.
50. Tsuji, S., et al., *Secretion of intelectin-1 from malignant pleural mesothelioma into pleural effusion.* Br J Cancer, 2010. **103**(4): p. 517-23.
51. Zheng, L., et al., *Aberrant expression of intelectin-1 in gastric cancer: its relationship with clinicopathological features and prognosis.* J Cancer Res Clin Oncol, 2012. **138**(1): p. 163-72.
52. Mogal, A.P., et al., *Haploinsufficient prostate tumor suppression by Nkx3.1: a role for chromatin accessibility in dosage-sensitive gene regulation.* J Biol Chem, 2007. **282**(35): p. 25790-800.
53. Li, D., et al., *Intelectin 1 suppresses the growth, invasion and metastasis of neuroblastoma cells through up-regulation of N-myc downstream regulated gene 2.* Molecular Cancer, 2015. **14**(1): p. 47.
54. Whilde, J., M.Q. Martindale, and D.J. Duffy, *Precision wildlife medicine: applications of the human-centred precision medicine revolution to species conservation.* Global Change Biology, 2017. **23**(5): p. 1792-1805.
55. Worst, B.C., et al., *Next-generation personalised medicine for high-risk paediatric cancer patients – The INFORM pilot study.* European Journal of Cancer, 2016. **65**: p. 91-101.
56. Duffy, D.J., *Problems, challenges and promises: perspectives on precision medicine.* Briefings in Bioinformatics, 2016. **17**(3): p. 494-504.
57. Duffy, D.J., et al., *GSK3 Inhibitors Regulate MYCN mRNA Levels and Reduce Neuroblastoma Cell Viability through Multiple Mechanisms, Including p53 and Wnt Signaling.* Molecular Cancer Therapeutics, 2014. **13**(2): p. 454-467.
58. Duffy, D.J., et al., *Integrative omics reveals MYCN as a global suppressor of cellular signalling and enables network-based therapeutic target discovery in neuroblastoma.* Oncotarget, 2015. **6**(41): p. 43182-43201.
59. Schwarzl, T., *Measuring transcription rate changes via time-course 4-thiouridine pulse-labelling improves transcriptional target identification.* J Mol Biol, 2015. **427**.
60. McMorris, F.A. and F. Ruddle, *Expression of neuronal phenotypes in neuroblastoma cell hybrids.* Developmental biology, 1974. **39**(2): p. 226-246.
61. Rosenbloom, K.R., et al., *The UCSC Genome Browser database: 2015 update.* Nucleic Acids Research, 2015. **43**(D1): p. D670-D681.
62. Murdoch, J.N., et al., *Sequence and expression analysis of Nhlh 1: a basic helix-loop-helix gene implicated in neurogenesis.* Developmental genetics, 1999. **24**(1-2): p. 165-177.
63. Brown, L., et al., *HEN1 and HEN2: a subgroup of basic helix-loop-helix genes that are coexpressed in a human neuroblastoma.* Proceedings of the National Academy of Sciences, 1992. **89**(18): p. 8492-8496.
64. Isogai, E., et al., *Oncogenic LMO3 Collaborates with HEN2 to Enhance Neuroblastoma Cell Growth through Transactivation of Mash1.* PLOS ONE, 2011. **6**(5): p. e19297.
65. Zhang, W., et al., *Comparison of RNA-seq and microarray-based models for clinical endpoint prediction.* Genome Biology, 2015. **16**(1): p. 133.
66. Domingo-Fernandez, R., et al., *The role of genetic and epigenetic alterations in neuroblastoma disease pathogenesis.* Pediatric Surgery International, 2012: p. 1-19.
67. Harenza, J.L., et al., *Transcriptomic profiling of 39 commonly-used neuroblastoma cell lines.* Scientific Data, 2017. **4**: p. 170033.
68. Forbes, S.A., et al., *COSMIC: somatic cancer genetics at high-resolution.* Nucleic Acids Research, 2017. **45**(D1): p. D777-D783.
69. Mayor, R. and E. Theveneau, *The role of the non-canonical Wnt–planar cell polarity pathway in neural crest migration.* Biochemical Journal, 2014. **457**: p. 19-26.
70. Michaelidis, T. and D. Lie, *Wnt signaling and neural stem cells: caught in the Wnt web.* Cell and Tissue Research, 2008. **331**(1): p. 193-210.
71. Leung, A.W., et al., *WNT/β-catenin signaling mediates human neural crest induction via a pre-neural border intermediate.* Development, 2016. **143**(3): p. 398-410.
72. Blanc, E., et al., *Low expression of Wnt-5a gene is associated with high-risk neuroblastoma.* Oncogene, 2005. **24**(7): p. 1277.
73. Anastas, J.N. and R.T. Moon, *WNT signalling pathways as therapeutic targets in cancer.* Nat Rev Cancer, 2013. **13**(1): p. 11-26.
74. Eleveld, T.F., et al., *Relapsed neuroblastomas show frequent RAS-MAPK pathway mutations.* Nature Genetics, 2015. **47**: p. 864–871
75. Padovan-Merhar, O.M., et al., *Enrichment of Targetable Mutations in the Relapsed Neuroblastoma Genome.* PLOS Genetics, 2016. **12**(12): p. e1006501.
76. Gao, B., et al., *Wnt Signaling Gradients Establish Planar Cell Polarity by Inducing Vangl2 Phosphorylation through Ror2.* Developmental Cell, 2011. **20**(2): p. 163-176.
77. Dreidax, D., et al., *p19-INK4d inhibits neuroblastoma cell growth, induces differentiation and is hypermethylated and downregulated in MYCN-amplified neuroblastomas.* Human Molecular Genetics, 2014. **23**(25): p. 6826-6837.

78. Cohn, S.L., et al., *The International Neuroblastoma Risk Group (INRG) Classification System: An INRG Task Force Report.* Journal of Clinical Oncology, 2009. **27**(2): p. 289-297.
79. Huang, M. and W.A. Weiss, *Neuroblastoma and MYCN.* Cold Spring Harbor Perspectives in Medicine, 2013. **3**(10).
80. Greene, C.S., et al., *Understanding multicellular function and disease with human tissue-specific networks.* Nat Genet, 2015. **47**(6): p. 569-576.
81. Barone, G., et al., *New Strategies in Neuroblastoma: Therapeutic Targeting of MYCN and ALK.* Clinical Cancer Research, 2013. **19**(21): p. 5814-5821.
82. Kumar, R., et al., *Design, synthesis of allosteric peptide activator for human SIRT1 and its biological evaluation in cellular model of Alzheimer's disease.* European journal of medicinal chemistry, 2017. **127**: p. 909-916.
83. Santo, E.E., et al., *Oncogenic activation of FOXR1 by 11q23 intrachromosomal deletion-fusions in neuroblastoma.* Oncogene, 2012. **31**(12): p. 1571-1581.
84. Blanc, E., et al., *Wnt-5a gene expression in malignant human neuroblasts.* Cancer Letters, 2005. **228**(1): p. 117-123.
85. Chen, Y., et al., *Oncogenic mutations of ALK kinase in neuroblastoma.* Nature, 2008. **455**(7215): p. 971.
86. Zhu, S., et al., *Activated ALK Collaborates with MYCN in Neuroblastoma Pathogenesis.* Cancer Cell, 2012. **21**(3): p. 362-373.
87. Schwarzl, T., et al., *Measuring Transcription Rate Changes via Time-Course 4-Thiouridine Pulse-Labelling Improves Transcriptional Target Identification.* Journal of Molecular Biology, 2015. **427**(21): p. 3368-3374.
88. Salm, F., et al., *RNA interference screening identifies a novel role for autocrine fibroblast growth factor signaling in neuroblastoma chemoresistance.* Oncogene, 2013. **32**(34): p. 3944-3953.

Figure Legends

Figure 1. Identification of a VANGL2-ITLN1 fusion gene in IMR32 cells. (A) Schematic overview of the VANGL2-ITLN1 fusion transcript. **(B)** Level of absolute gene expression of VANGL2 and ITLN1 mRNA transcripts across five neuroblastoma cell lines as detected by RNA-seq. Expression is in read counts per million adjusted by gene length in kilobases (CPMkb), with error bars denoting the standard deviation between replicates. **(C)** Relative expression of VANGL2-ITLN1 fusion gene and the wild type VANGL2 and ITLN1transcripts in IMR32 cells, as detected by RT-qPCR. Error bars denote RQ Min and RQ Max, and the levels of expression for each gene are set relative to those of the fusion gene. **(D)** Relative expression of the fusion components (VANGL2 and ITLN1) genes' immediate upstream and downstream genomic neighbours, as detected by RNA-seq. Depicted is the relative change in expression level of each gene in IMR32 compared with the average expression of that gene in four other neuroblastoma cell lines (SY5Y, Kelly, KCN and KCNR).

Figure 2. Patient outcome segregated by VANGL2 and ITLN1 expression. (A) Kaplan-Meier survival curves showing the predictive strength of the expression levels of the fusion gene components VANGL2 and ITLN1 mRNAs in neuroblastoma tumours on patient outcome. Curves generated using the SEQC [65] 498 neuroblastoma tumour dataset in the R2: Genomics Analysis and Visualization Platform (http://r2.amc.nl). For the ITLN1 high and low expression cut-off value for the ITLN1 Kaplan-Meier survival curve please see supplementary table 3 (Table S3).

Figure 3. Patient outcome segregated by ITLN1 expression, for discrete neuroblastoma stages and MYCN status. (A) ITLN1 mRNA expression level across a large cohort of neuroblastoma tumours. Results are grouped by tumour stage, with the risk status, MYCN

amplification status and International Neuroblastoma Staging System (INSS) stage of each tumour indicated. **(B)** Kaplan-Meier survival curves separated by neuroblastoma tumour stage, showing the predictive strength of the expression levels of the ITLN1 mRNA for patient outcome. **(C)** Kaplan-Meier survival curves separated by a tumour's MYCN amplification status, showing the predictive strength of the expression levels of the ITLN1 mRNA for patient outcome. All panels generated using the SEQC [65] 498 neuroblastoma tumour dataset in the R2: Genomics Analysis and Visualization Platform (http://r2.amc.nl). For the ITLN1 high and low expression cut-off values for each of the the ITLN1 Kaplan-Meier survival curves (Fig. 3B, C) please see supplementary table 3 (Table S3).

Figure 4. VANGL2 and ITLN1 expression in a large panel of neuroblastoma cell lines and Wnt5A as a predictor of neuroblastoma patient outcome. (A) VANGL2 and ITLN1 expression across the 39 neuroblastoma cell lines and two control non-neuroblastoma samples (human foetal brain tissue and RPE1 cells, a retinal pigment epithelial cell line) profiled by RNA-seq by Harenza *et al.* (2017) [67], expression measured in FPKMBs. **(B)** VANGL2 (top) and ITLN1 (bottom) expression across a large cohort of human healthy tissue samples (shaded green) and malignant tissue samples (shaded red). The number of individual samples per tissue type is shown in brackets in each x-axis label. The data relating to expression in the neuroblastoma sample cohort is highlighted by a red arrow. Expression data obtained from and graph generated using the *In Silico* Transcriptomics (IST) Online database (http://ist.medisapiens.com/, version 2.1.3). **(C)** VANGL2 and ITLN1 expression across a large panel of cell lines. Expression data obtained from and graph generated using the IST Online database (http://ist.medisapiens.com/, version 2.1.3). **(D)** Kaplan-Meier survival curves showing the predictive strength of the expression level of WNT5 mRNA in neuroblastoma tumours on patient outcome. Curves generated using the SEQC [65] 498 neuroblastoma tumour dataset in the R2: Genomics Analysis and Visualization Platform (http://r2.amc.nl).

Figure 5. Molecular interactions between the VANGL2-ITLN1 fusion gene components and the MYCN and Wnt signalling networks. (A) Right: relative expression of VANGL2 and ITLN1 mRNA (fusion and wild types not resolved by RNA-seq) in untreated and 28mM lithium chloride treated IMR32 cells, as detected by RNA-seq. Absolute expression levels measured in CPMkb are inset within each bar. Error bars denote the standard deviation between replicates, and the levels of expression for each gene are set relative to those in the untreated control cells. Left: relative expression of VANGL2-ITLN1 fusion gene and wild type VANGL2 and ITLN1 mRNA in untreated and 28mM lithium chloride treated IMR32 cells, as detected by qPCR. Error bars denote the RQ Min and RQ Max between replicates, and the levels of expression for each transcript are set relative to those in the untreated control cells. **(B)** Interaction network between VANGL2, ITLN1 and MYCN pathway component genes, generated using the GIANT (http://giant.princeton.edu/) database. **(C)** Schematic overview of putative multi-level MYCN, ITLN1 and VANGL2 interactions in neuroblastoma cells. Proteins are denoted by (p), while genomic DNA is denoted by (g).

Supplemental Figure Legends

Supplemental Figure 1. Additional gene expression and focus formation assay data. (A) Level of absolute gene expression of WNT5A mRNA transcripts across our five neuroblastoma cell line panel (left), and the Harenza *et al.* (2017) [67] 39 neuroblastoma cell line panel (right). Expression is in CPMkb (left) and FPKMBs (right). **(B)** Protein-protein interactions between VANGL2 and Wnt pathway component genes, generated using the String database (v10.5, www.string-db.org). **(C)** NIH-3T3 mouse fibroblasts focus formation assay for transfection with VANGL2-ITLN1 expressing plasmid, H-Ras12V plasmid (0.03 µg/ml) was used as a positive control, while empty vector, GFP plasmid (0.2 µg/ml) and reverse orientation VANGL2-ITLN1 plasmid (0.4 µg/ml) were used as negative controls. Forward orientation VANGL2-ITLN1 plasmid was also transfected at a concentration of 0.4 µg/ml. Plates were imaged 4 weeks (3 weeks for the H-Ras12V control cells) after transfection. **(D)** Relative expression level of VANGL2-ITLN1 transcript above plasmid background in NIH-3T3 cells transfected with empty vector, forward orientation VANGL2-ITLN1 plasmid or reverse orientation VANGL2-ITLN1 plasmid, as detected by RT-qPCR.

Supplemental Figure 2. Additional ITLN and VANGL2 MYCN interaction data. (A) Mass spectrometry LFQ intensity values for MYCN co-immunoprecipitation (coIP) showing the detection of ITLN (ITLN1 and ITLN2 peptides upon 24h of doxycycline induced MYCN overexpression in SY5Y-MYCN cells (left). LFQ intensity values for positive control MYCN-MYCN coIP (left). Note: MYCN reaches supraphysiological levels upon overexpression in SY5Y-MYCN cells compared with non-transformed cells. However, the level of expression achieved in SY5Y-MYCN is only equivalent to that of neuroblastoma cells with modest MYCN amplification [58]. Highly amplified MYCN express MYCN at even more highly elevated levels [58]. Therefore, while the MYCN expression in induced SY5Y-MYCN is well above the level seen in normal untransformed cells, it is in the physiological range experienced by MYCN-amplified neuroblastoma tumours. **(B)** Relative expression level of VANGL2 mRNA after 4h MYCN overexpression in the SY5Y-MYCN, MYCN inducible cell line, as detected by 4-Thiouridine Pulse-Labelling RNA-seq (4sU-seq). Error bars denote the standard deviation between replicates, and the level of VANGL2 expression is set relative to that of un-induced control cells.

Table S3. The ITLN1 high and low expression cut-off values for each of the ITLN1 Kaplan-Meier survival curves, Figs 2A, 3B, C. These curves and cut-offs were generated using the scan cut-off Kaplan-Meier survival curves function of the R2: Genomics Analysis and Visualization Platform (http://r2.amc.nl) applied to the SEQC [65] 498 neuroblastoma tumour dataset.

SEQC 498 NB tumour dataset	ITLN1 expression cut-off value
Entire dataset	1.010
Stage 1 & 2	1.010
Stage 3	1.010
Stage 4	1.105
Stage 4S	1.088
MYCN amplified	1.105
MYCN non-amplified	1.204

Figure 1

A

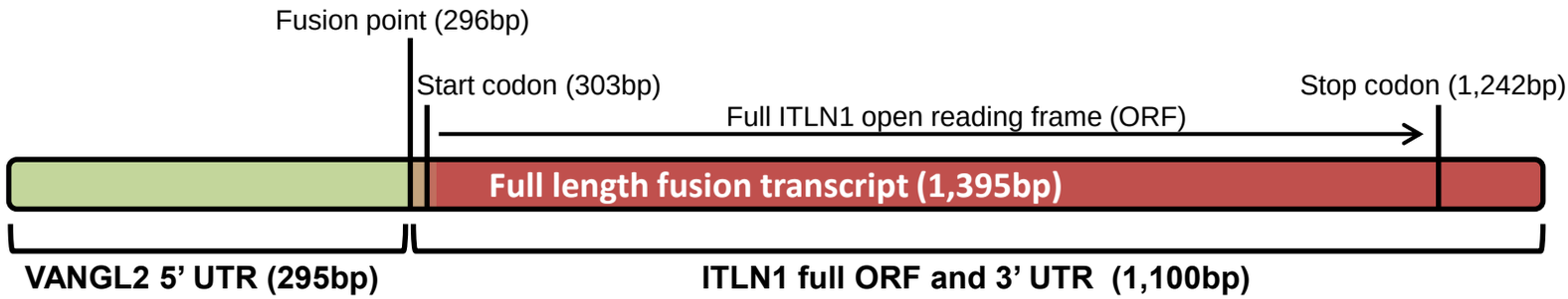

B

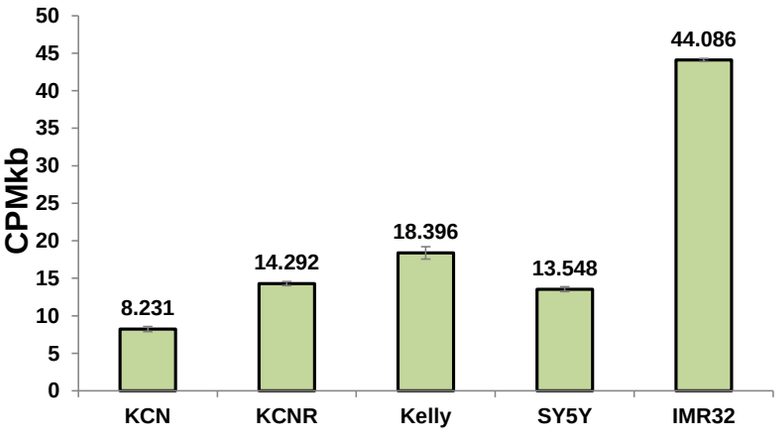

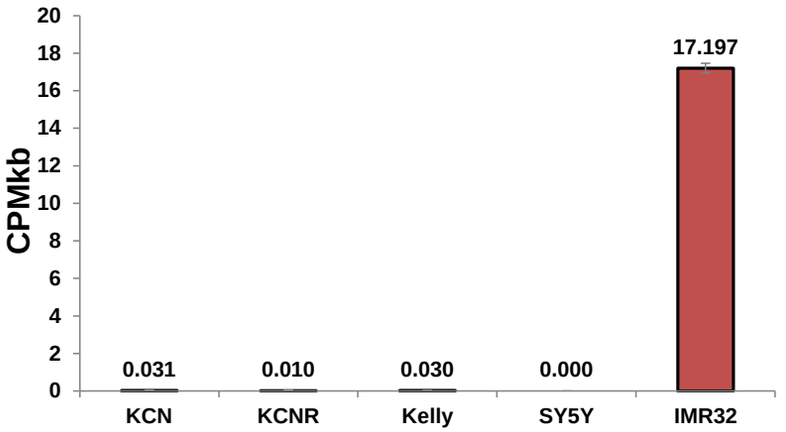

C

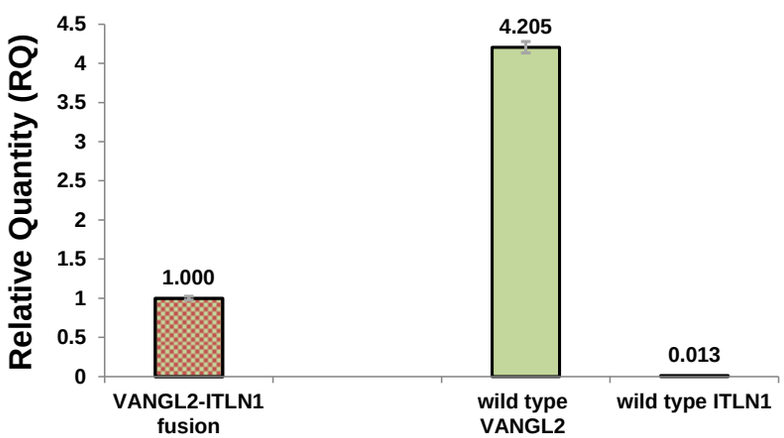

D

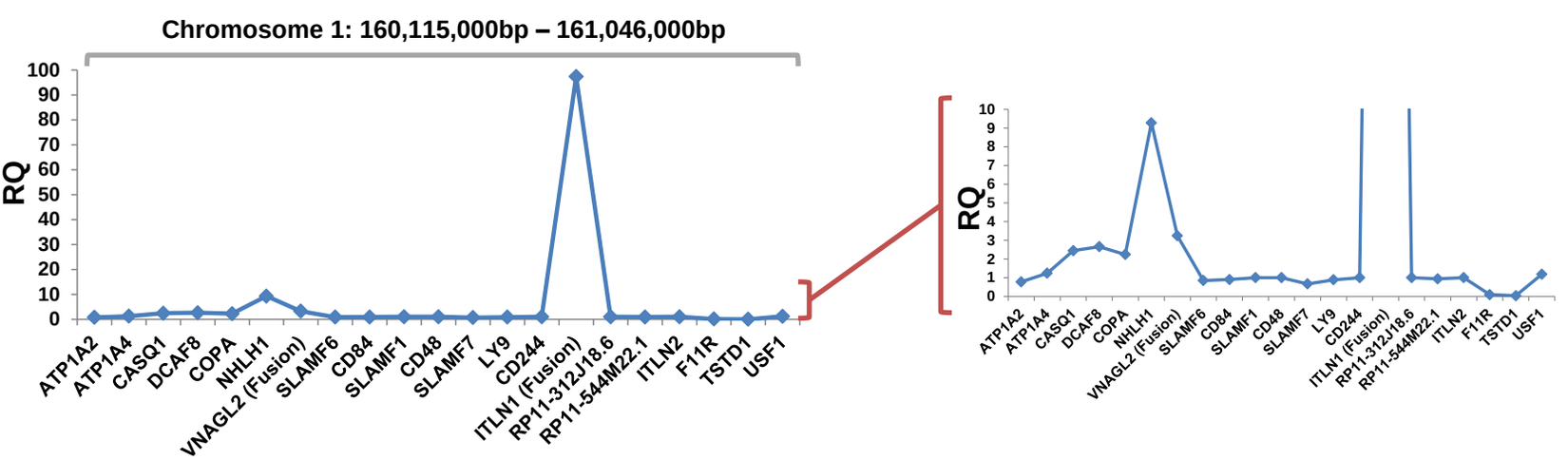

Figure 2

A

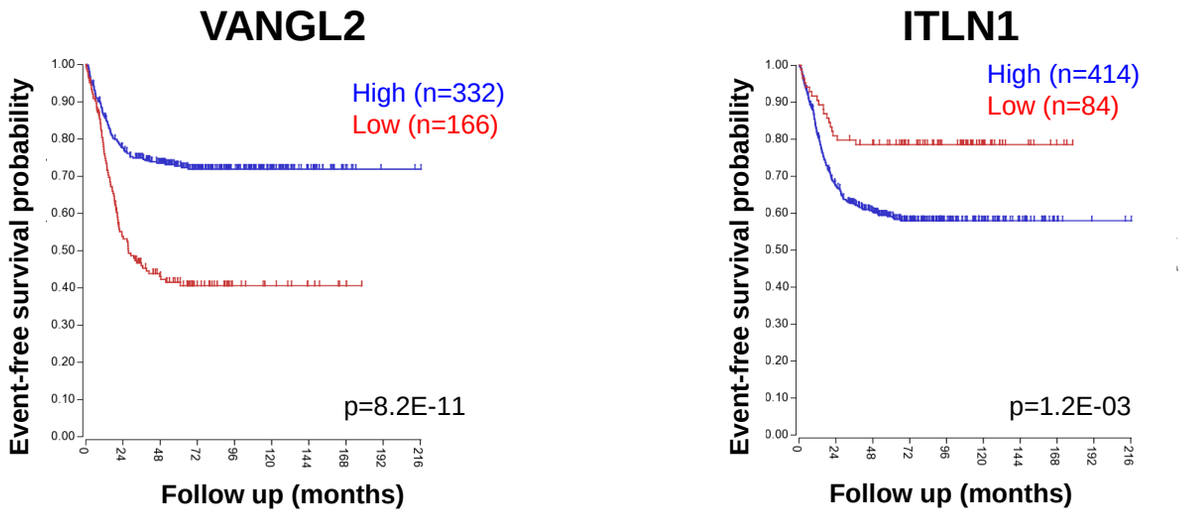
VANGL2
High (n=332)
Low (n=166)
p=8.2E-11
Event-free survival probability
Follow up (months)
ITLN1
High (n=414)
Low (n=84)
p=1.2E-03
Event-free survival probability
Follow up (months)

Figure 3

A

ITLN1 expression per tumour stage

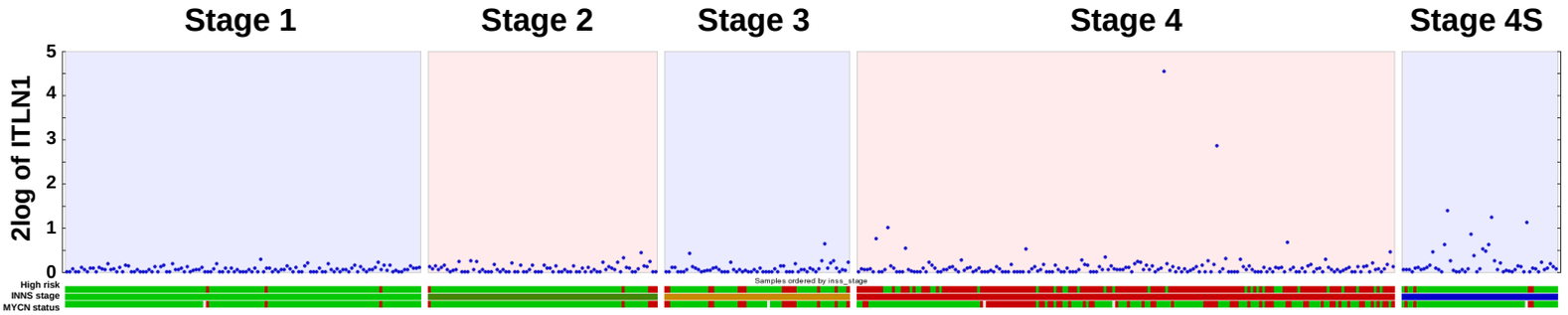

B

ITLN1 by tumour stage

Stage 1 & 2 tumours

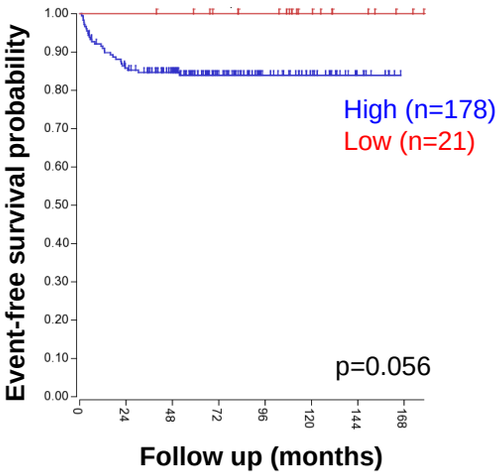

Stage 3 tumours

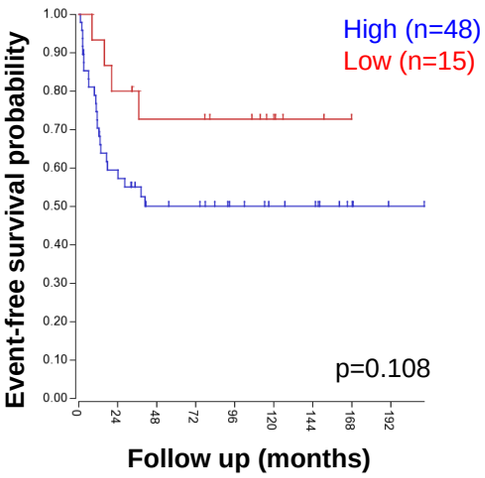

Stage 4 tumours

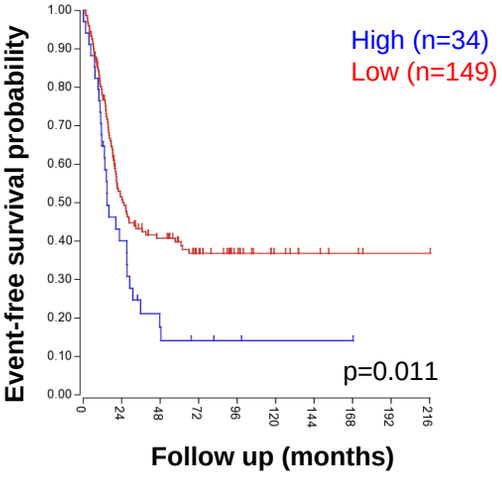

Stage 4S tumours

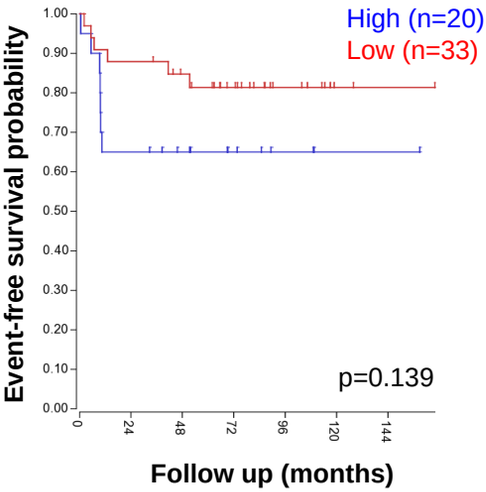

C

ITLN1 by MYCN amplification status

MYCN non- amplified tumours

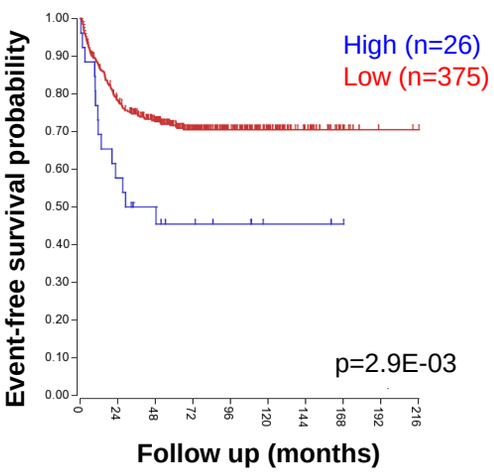

MYCN amplified tumours

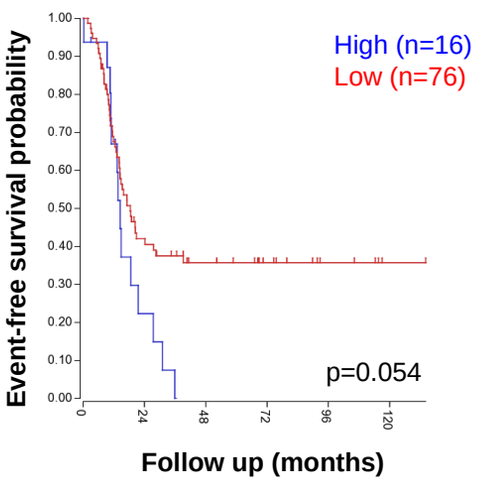

Figure 4

A

VANGL2 mRNA (NB cell line panel)

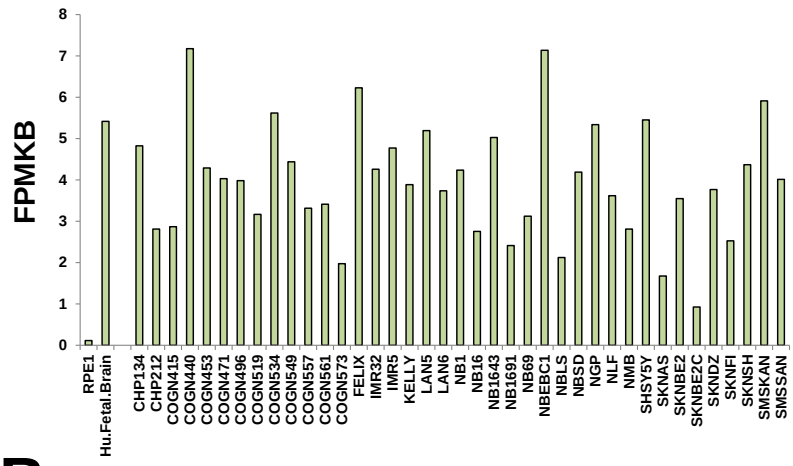

ITLN1 mRNA (NB cell line panel)

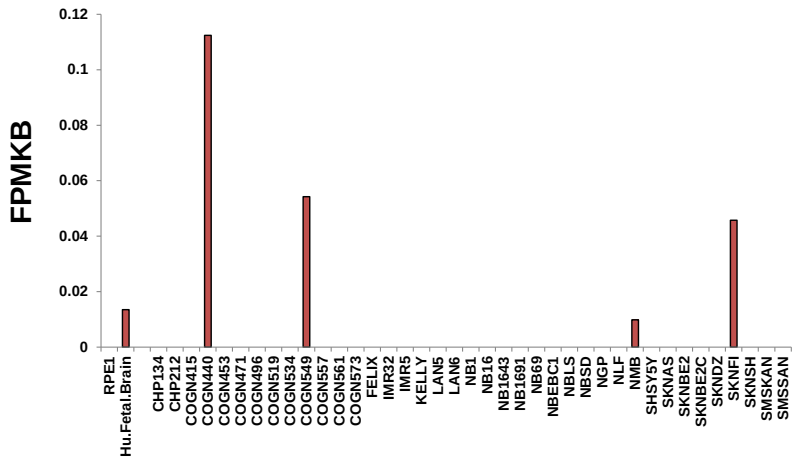

B

VANGL2 mRNA (tissue panel)

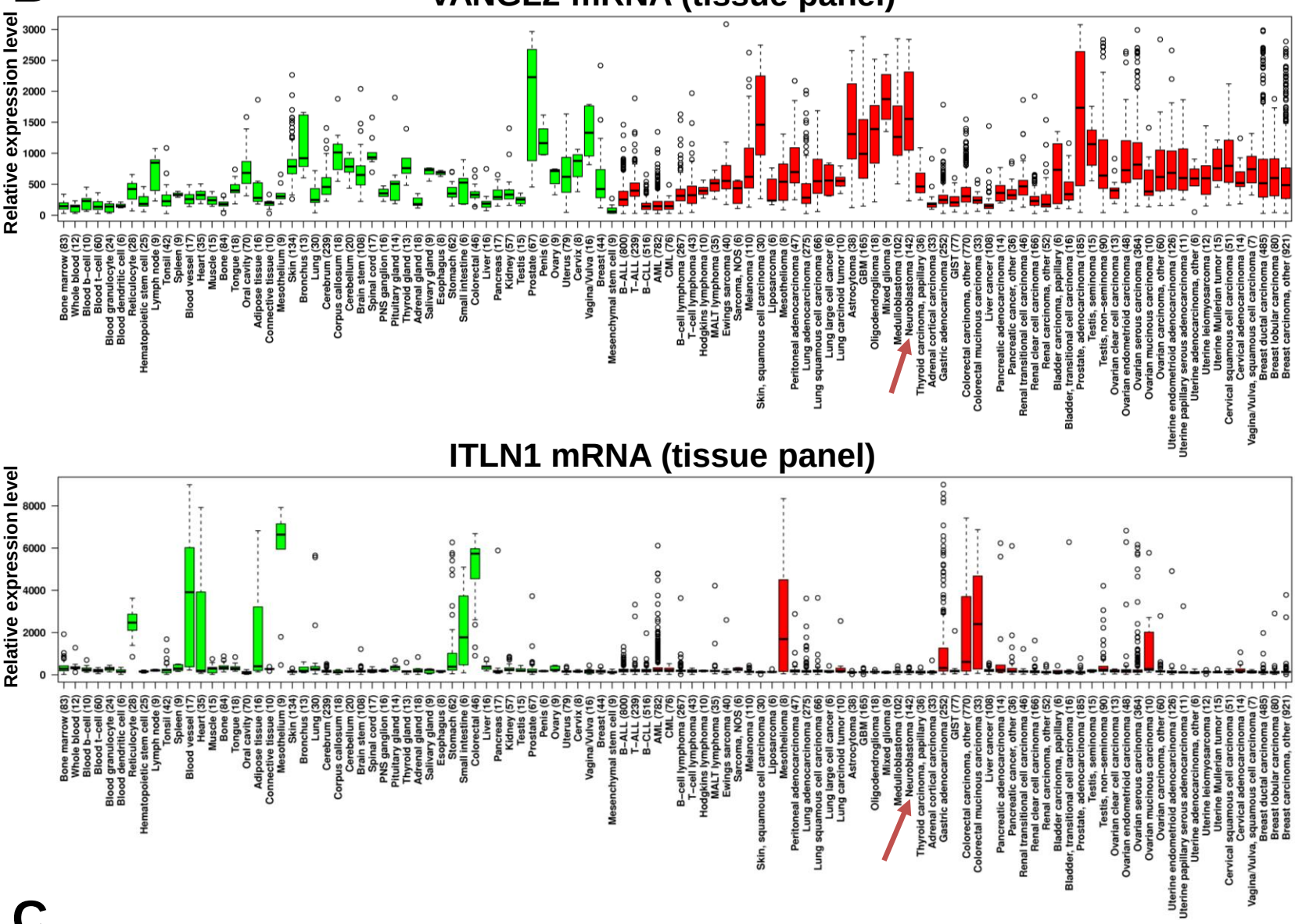

ITLN1 mRNA (tissue panel)

C

VANGL2 mRNA (cell line panel)

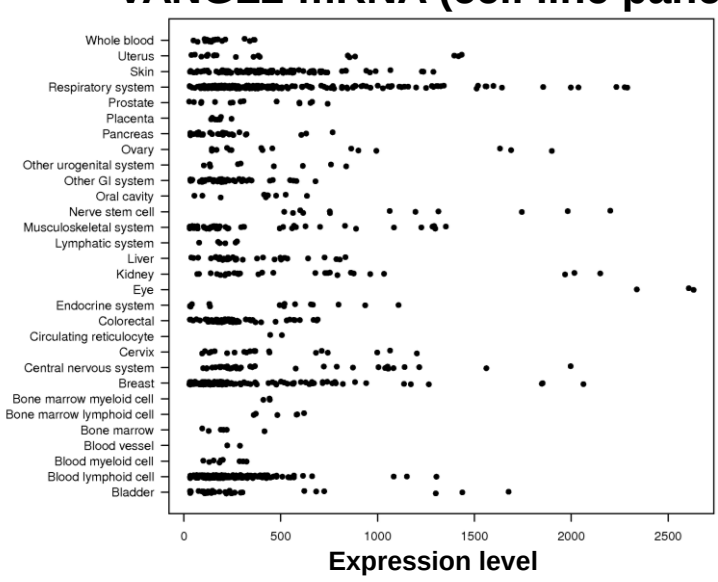

ITLN1 mRNA (cell line panel)

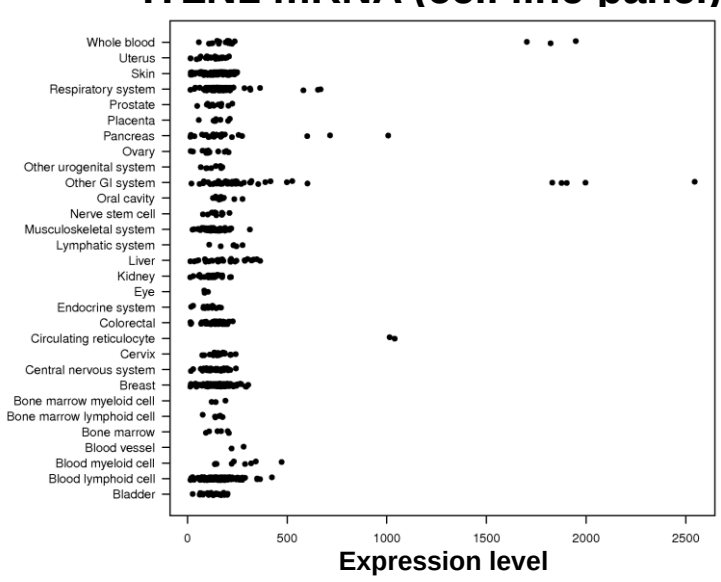

D

WNT5A

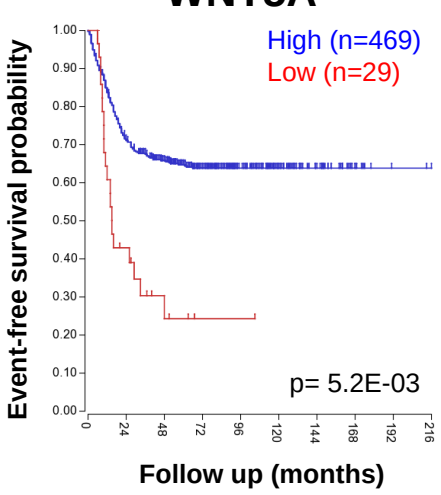

Figure 5

A

VANGL2 and ITLN1 mRNAs upon GSK3β inhibition (IMR32)

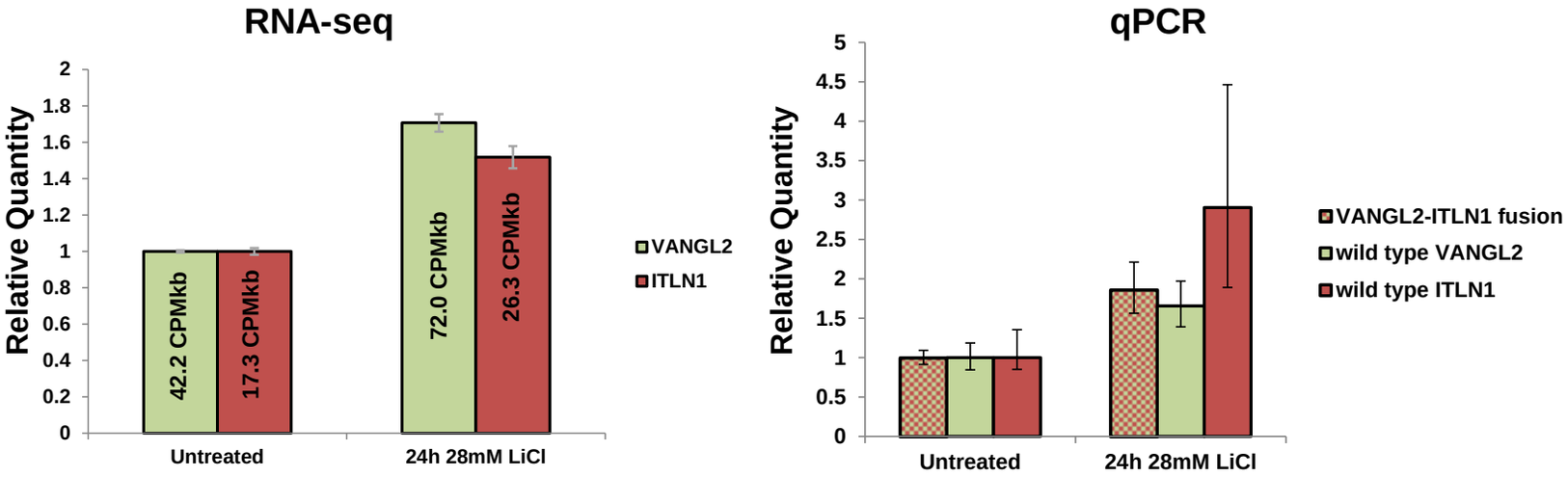

B

MYCN, ITLN1, and VANGL2 gene network analysis

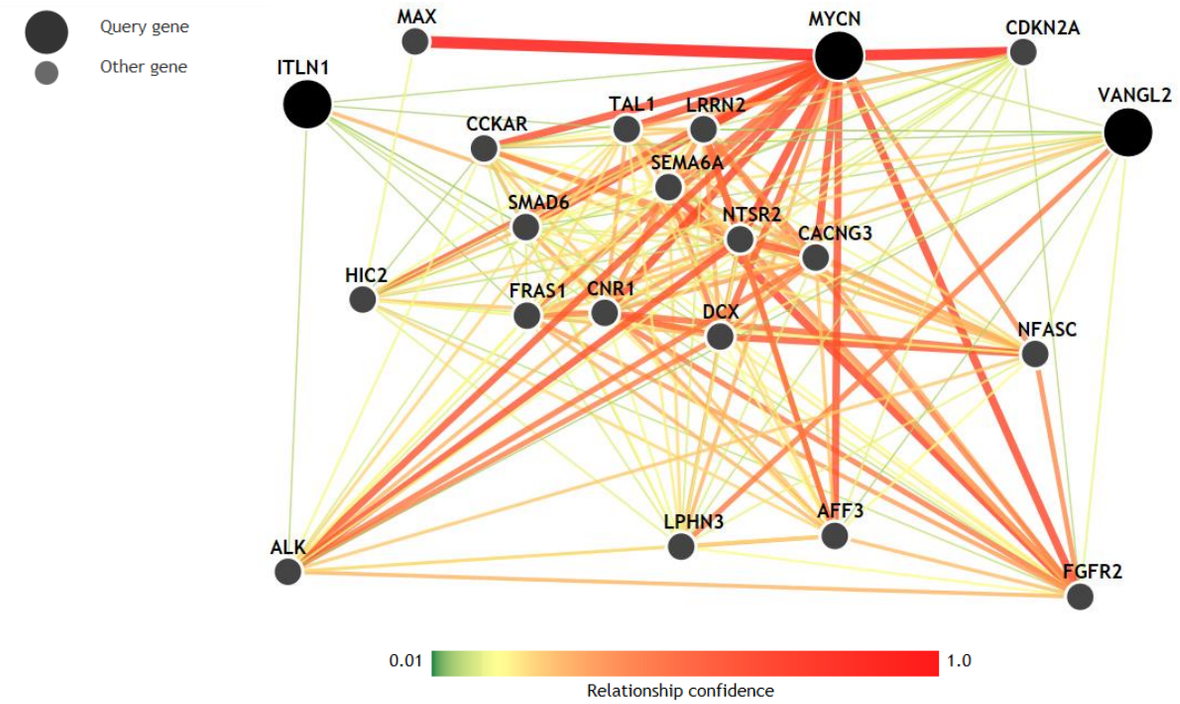

C

MYCN, ITLN1, VANGL2 interactions in neuroblastoma cells (ChIP-seq, 4sU-seq and coIP)

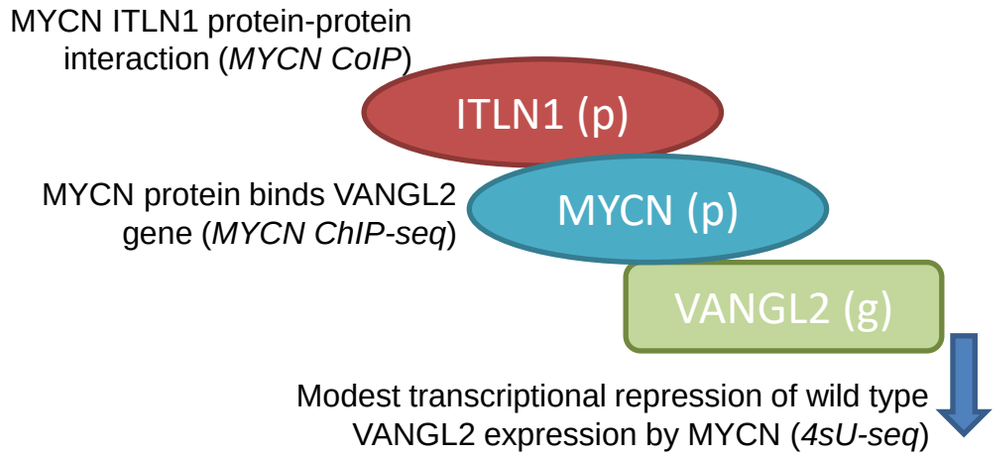

Figure S1

A

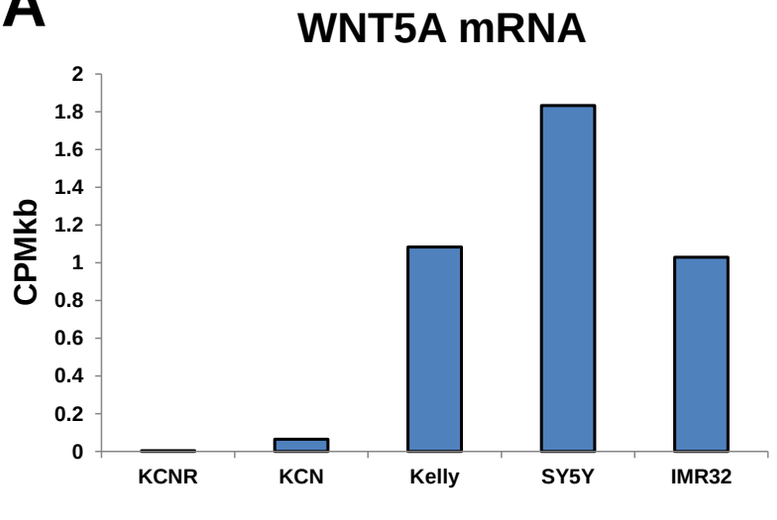

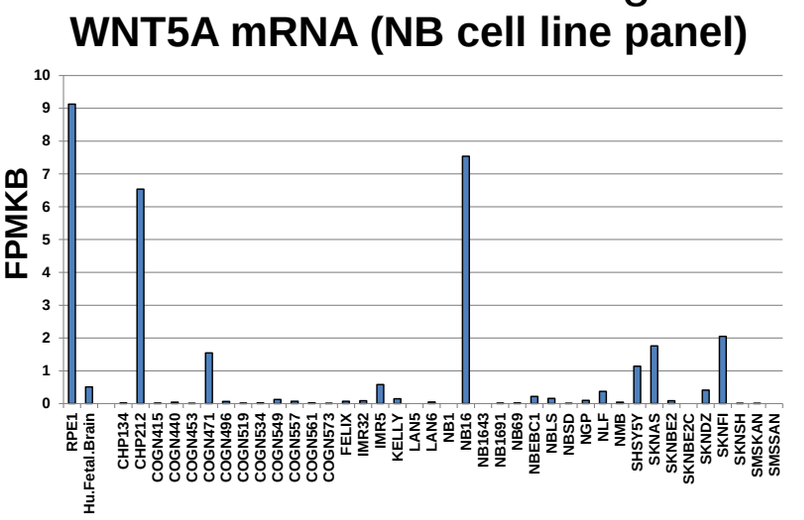

B

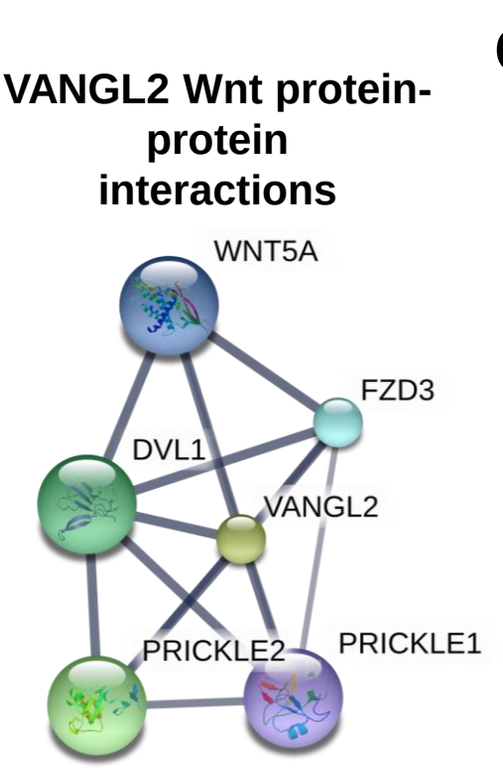

C

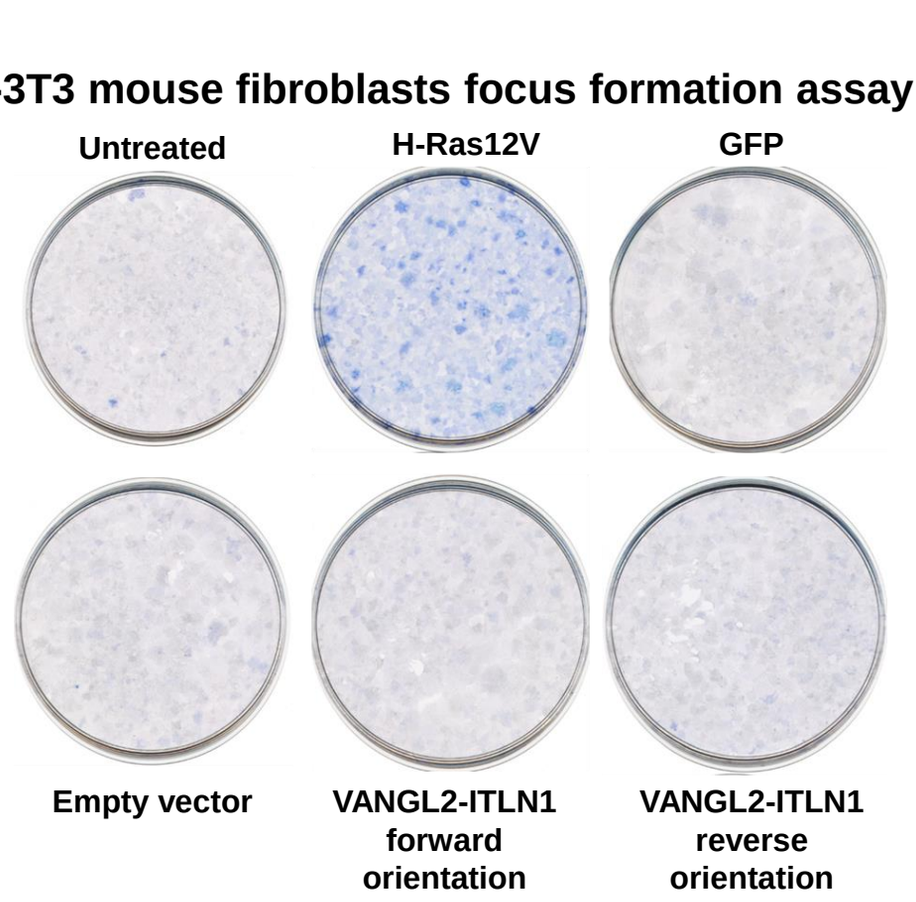

D

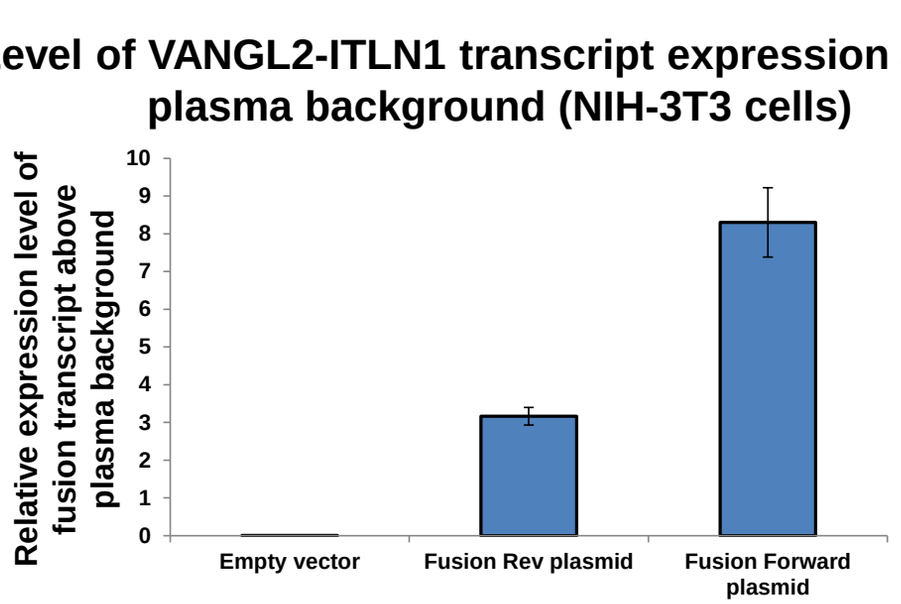

A

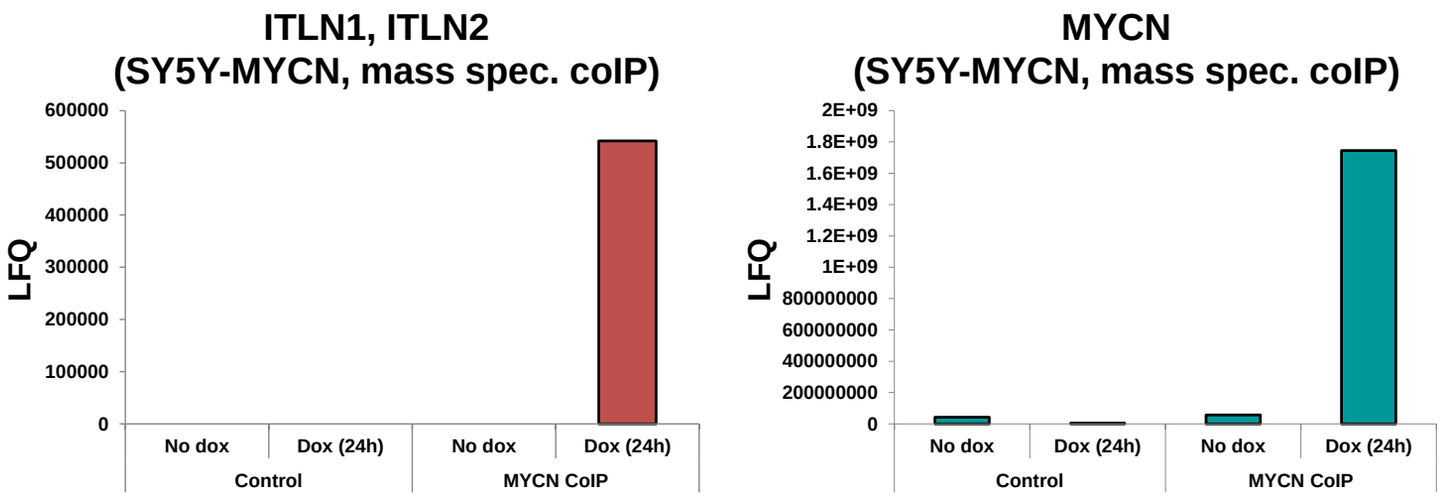
ITLN1, ITLN2
(SY5Y-MYCN, mass spec. coIP)
LFQ
600000
500000
400000
300000
200000
100000
0
No dox
Dox (24h)
No dox
Dox (24h)
Control
MYCN CoIP
MYCN
(SY5Y-MYCN, mass spec. coIP)
LFQ
2E+09
1.8E+09
1.6E+09
1.4E+09
1.2E+09
1E+09
800000000
600000000
400000000
200000000
0
No dox
Dox (24h)
No dox
Dox (24h)
Control
MYCN CoIP

B

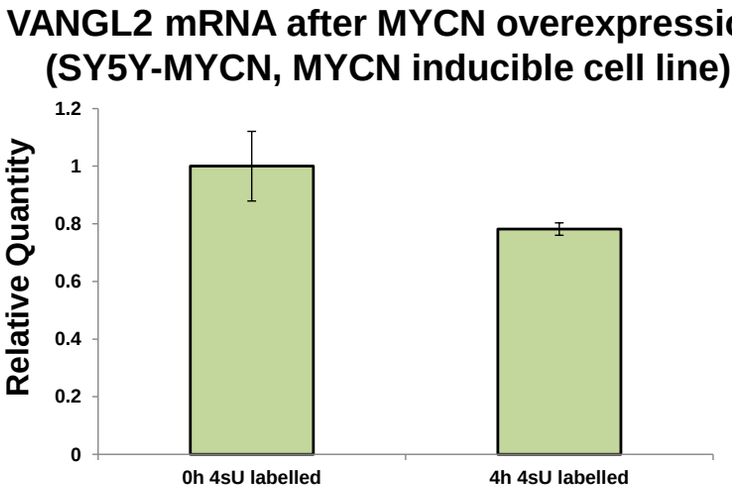
VANGL2 mRNA after MYCN overexpression
(SY5Y-MYCN, MYCN inducible cell line)
Relative Quantity
1.2
1
0.8
0.6
0.4
0.2
0
0h 4sU labelled
4h 4sU labelled

Supplemental Figure Legends

Supplemental Figure 1. Additional gene expression and focus formation assay data. (A) Level of absolute gene expression of WNT5A mRNA transcripts across our five neuroblastoma cell line panel (left), and the Harenza *et al.* (2017) [67] 39 neuroblastoma cell line panel (right). Expression is in CPMkb (left) and FPKMBs (right). **(B)** Protein-protein interactions between VANGL2 and Wnt pathway component genes, generated using the String database (v10.5, www.string-db.org). **(C)** NIH-3T3 mouse fibroblasts focus formation assay for transfection with VANGL2-ITLN1 expressing plasmid, H-Ras12V plasmid (0.03 µg/ml) was used as a positive control, while empty vector, GFP plasmid (0.2 µg/ml) and reverse orientation VANGL2-ITLN1 plasmid (0.4 µg/ml) were used as negative controls. Forward orientation VANGL2-ITLN1 plasmid was also transfected at a concentration of 0.4 µg/ml. Plates were imaged 4 weeks (3 weeks for the H-Ras12V control cells) after transfection. **(D)** Relative expression level of VANGL2-ITLN1 transcript above plasmid background in NIH-3T3 cells transfected with empty vector, forward orientation VANGL2-ITLN1 plasmid or reverse orientation VANGL2-ITLN1 plasmid, as detected by RT-qPCR.

Supplemental Figure 2. Additional ITLN and VANGL2 MYCN interaction data. (A) Mass spectrometry LFQ intensity values for MYCN co-immunoprecipitation (coIP) showing the detection of ITLN (ITLN1 and ITLN2 peptides upon 24h of doxycycline induced MYCN overexpression in SY5Y-MYCN cells (left). LFQ intensity values for positive control MYCN-MYCN coIP (left). Note: MYCN reaches supraphysiological levels upon overexpression in SY5Y-MYCN cells compared with non-transformed cells. However, the level of expression achieved in SY5Y-MYCN is only equivalent to that of neuroblastoma cells with modest MYCN amplification [58]. Highly amplified MYCN express MYCN at even more highly elevated levels [58]. Therefore, while the MYCN expression in induced SY5Y-MYCN is well above the level seen in normal untransformed cells, it is in the physiological range experienced by MYCN-amplified neuroblastoma tumours. **(B)** Relative expression level of VANGL2 mRNA after 4h MYCN overexpression in the SY5Y-MYCN, MYCN inducible cell line, as detected by 4-Thiouridine Pulse-Labelling RNA-seq (4sU-seq). Error bars denote the standard deviation between replicates, and the level of VANGL2 expression is set relative to that of un-induced control cells.

Supplemental Table

Table S3. The ITLN1 high and low expression cut-off values for each of the ITLN1 Kaplan-Meier survival curves, Figs 2A, 3B, C. These curves and cut-offs were generated using the scan cut-off Kaplan-Meier survival curves function of the R2: Genomics Analysis and Visualization Platform (http://r2.amc.nl) applied to the SEQC [65] 498 neuroblastoma tumour dataset.

SEQC 498 NB tumour dataset	ITLN1 expression cut-off value
Entire dataset	1.010
Stage 1 & 2	1.010
Stage 3	1.010
Stage 4	1.105
Stage 4S	1.088
MYCN amplified	1.105
MYCN non-amplified	1.204